Studies on the formation mechanism of zinc protoporphyrin IX from the heme proteins *via* their heme dissociation in the nitrite/nitrate-free meat products

（亜硝酸塩/硝酸塩無添加食肉製品中におけるヘムの解離を介したヘムタンパク質からの亜鉛プロトポルフィリン IX 形成機構に関する研究）

Hokkaido University, Graduate School of Agriculture
Division of Frontiers in Bioscience, Doctor Course

Zhai Yang

翟　洋

Table of contents

Chapter 3 Investigating the inhibitory mechanism of nitrite on ZnPP formation in dry-cured meat product

Chapter 1

General introduction

1.1. Color of meat

Color is one of the most important factors of meat that influences consumer buying decision and affects their perception of the freshness of the meat (Tomasevic *et al.*, 2021). The myoglobin (Mb) is primarily responsible for the meat color (Boles & Pegg, 2010). Mb is a water-soluble protein, which consists of a globin and a non-proteinous porphyrin ring with a central iron atom. The defining factors of meat color are the ligands, such as oxygen (O_2) or water, bind with the heme iron and the electrovalence (ferrous or ferric) of the heme iron in Mb (Mancini & Hunt, 2005). The cut cross section of the fresh meat is quite dark or a deep purplish-red, and the pigment is mainly the deoxymyoglobin (DeoxyMb), which is a ferrous state of Mb and no ligand bind with its heme iron. As the O_2 from the air contacts with the exposed meat cross section, the O_2 ligand binds to the ferrous iron of the DeoxyMb to form the oxymyoglobin (OxyMb), which brings meat a bright cherry red color. When the DeoxyMb or the OxyMb lose an electron to be oxidized to the metmyoglobin (metMb), which contains the ferric iron and binds to the water ligand, the meat turns to a brown color. During meat storage without any color protection treatments, the meat will normally attain a dull brown color derived from metMb and influence consumer acceptance negatively (Carpenter *et al.*, 2001). Therefore, how to maintain an attractive color profile in meat during storage or processing has always been a subject of interest.

1.2. Color of meat products and its concerns by consumers

The use of synthetic nitrate and nitrite is very frequent in the meat processing industry for their color-fixative and other properties. Generally, cured meat products with the addition of nitrite/nitrate exhibit desirable bright red color owing to changes in the form of Mb. The nitric oxide (NO), which derives from the added nitrite/nitrate in meat, can react with the meat-endogenous Mb to form the nitrosyl myoglobin (NOMb) in the presence of endogenous or added reductants, and bring a relatively stable bright red color for the raw meat (Honikel, 2008). Even after heating, the cured meat still appears an

attractive color due to the formed NOMb being heat-denatured and converted to bright pink nitrosyl hemochrome (Parthasarathy & Bryan, 2012). In addition to the effect of nitrite on cured color development in meat products, it is strongly inhibitory to anaerobic bacteria, most importantly *Clostridium botulinum* and the outgrowth of its spores (Flores & Toldrá, 2021; Jin *et al.*, 2014), and contributes to the control of other microorganisms such as *Listeria monocytogenes* (Sebranek & Bacus, 2007). Moreover, the addition of nitrite can also improve the antioxidant properties (Bedale *et al.*, 2016) and retard the rancidity (Rivera *et al.*, 2019) of the cured meat products. NO may play an important role for this property because it can act as a free radical acceptor (Sato & Hegartv, 1971). Also, the antioxidant property of NO is reported that due to its ability to bind and stabilize heme iron of meat pigments, lowering the amount of free iron released during cooking, which is a potent catalyst of lipid oxidation in meat (Love & Pearson, 1974). On the other hand, nitrite is also responsible for the production of characteristic cured meat flavor, which may be due to the suppression of lipid oxidation by nitrite or the production of some volatile flavor factors by the reaction of nitrite with some components in cured meat (Sebranek & Bacus, 2007). Therefore, nitrite/nitrate are the preferable curing agents in the meat processing industry over the past several decades due to their various effects as well as improving the meat color.

However, the use of nitrite in meat products has been debated for several years due to its risk to form nitroso compounds, some of which are mutagenic. Many studies have suggested that the incidence of colorectal cancer due to the consumption of processed meat is closely related to the addition of sodium nitrite during the processing (Bouvard *et al.*, 2015; Cantwell & Elliott, 2017; Santarelli *et al.*, 2008). In fact, nitrite itself is not a carcinogen, but it results in the production of nitrosamine (a carcinogen) when it reacts with amines produced by the decomposition of proteins or when a product containing nitrite is heated at temperatures above 130℃ (Lee *et al.*, 2021; Sindelar & Milkowski, 2011). In order to reduce the hazard caused by excessive intake of nitrite to the human body, a joint food standard of FAO/WHO indicates when nitrite or nitrate (or a combination of both) in processed meat are used, it should not be residual in the final product to more than 200 mg/kg (World Health Organization, 2017). In addition, in the United States, it is regulated to contain less than 200 ppm of sodium nitrite and less than

500 ppm of sodium nitrate in the final meat products (Carey, 2020). However, since the requirements of consumers for organic and clean-label meat products have increased due to the concerns about the health risk of synthetic nitrite/nitrate, the meat industry has currently concerned with the development of nitrite/nitrate alternatives. To obtain the bacteriostatic and anti-oxidation effects comparable to nitrite implementation, some natural substances, such as herbs, spices, and organic acids were used as an alternative to nitrite/nitrate in cured meat products (Alahakoon *et al.*, 2015; Sebranek & Bacus, 2007). In contrast, it is hard to develop a favorable color in cured meat products without the addition of nitrite (Sebranek & Bacus, 2007), which influence consumer acceptance negatively. Therefore, some natural assuring treatments for reddening the dry-cured meat products without the addition of nitrite/nitrate is currently demanded.

1.3. Zinc protoporphyrin IX is the potential nitrite substitute for meat reddening

In traditional Italian Parma ham (*Prosciutto di Parma*), which is made from the legs of heavy pigs and matured over one year after curing with only sea salt, a stable bright red color is performed. According to the analysis using the absorption spectrum and the electron spin resonance spectrum, the lipophilic red pigment of Parma ham shows different characteristics from the NOMb, OxyMb, and Mb in other meats or cured meat products (Morita *et al.*, 1996). During the maturation of Parma ham, this red pigment gradually contributed to its bright red meat color rather than due to Mb or Mb derivatives (Møller *et al.*, 2003). After the mass spectrometric identification by Wakamatsu *et al.* (2004a), this red pigment in Parma ham was conformed as zinc protoporphyrin IX (ZnPP). The structure of ZnPP is similar to that of heme, which is the protoporphyrin IX (PPIX) with iron ions coordinated to the center, while ZnPP is PPIX with zinc ions coordinated to the center (Fig. 1). In Parma ham, about 60-70% of all porphyrins in were ZnPP, which was higher than that of heme (Taketani *et al.*, 2007; Wakamatsu *et al.*, 2009). The formation of ZnPP was also found in other nitrite-free dry-cured meat products, such as the dry-cured Iberian hams (Adamsen *et al.*, 2006) and the dry-cured fermented sausages (De Maere *et al.*, 2016). In addition, other meat sources besides pork, including chicken, turkey, lamb, beef, veal, and horse, also have the ability to produce ZnPP *in vitro* study (De Maere *et al.*, 2017). Moreover, the color stability of ZnPP in Parma ham against not

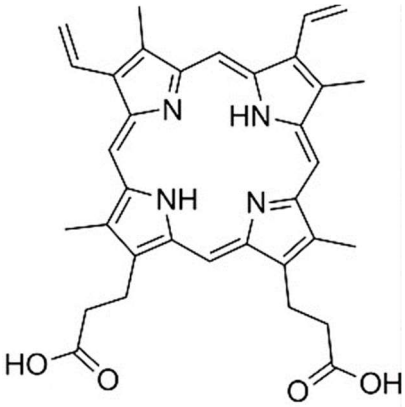

Protoporphyrin IX

(PPIX)

Zinc protoporphyrin IX

(ZnPP)

Fig. 1. The structure of protoporphyrin IX and zinc protoporphyrin IX

only light and heat but also low oxygen concentration (Adamsen *et al.*, 2004). Also, the formation of ZnPP in the dry-cured meat products, which were matured without nitrite/nitrate, has been reported to be positively correlated with the redness index (a*) of the meat color (Adamsen *et al.*, 2006; Parolari *et al.*, 2016). Therefore, ZnPP is considered as a potential pigment to improve the color of dry-cured meat products without adding nitrite/nitrate or any coloring agents.

1.4. The suggested pathway of ZnPP converted from the heme proteins in Parma ham

In recent years, many researches about the mechanism by which ZnPP is formed in the nitrite/nitrate-free dry-cured meat products were performed, and it has been proposed that ZnPP in Parma ham was formed through the conversion of heme, which came from the heme proteins, such as hemoglobin (Hb) and Mb (Fig. 2).

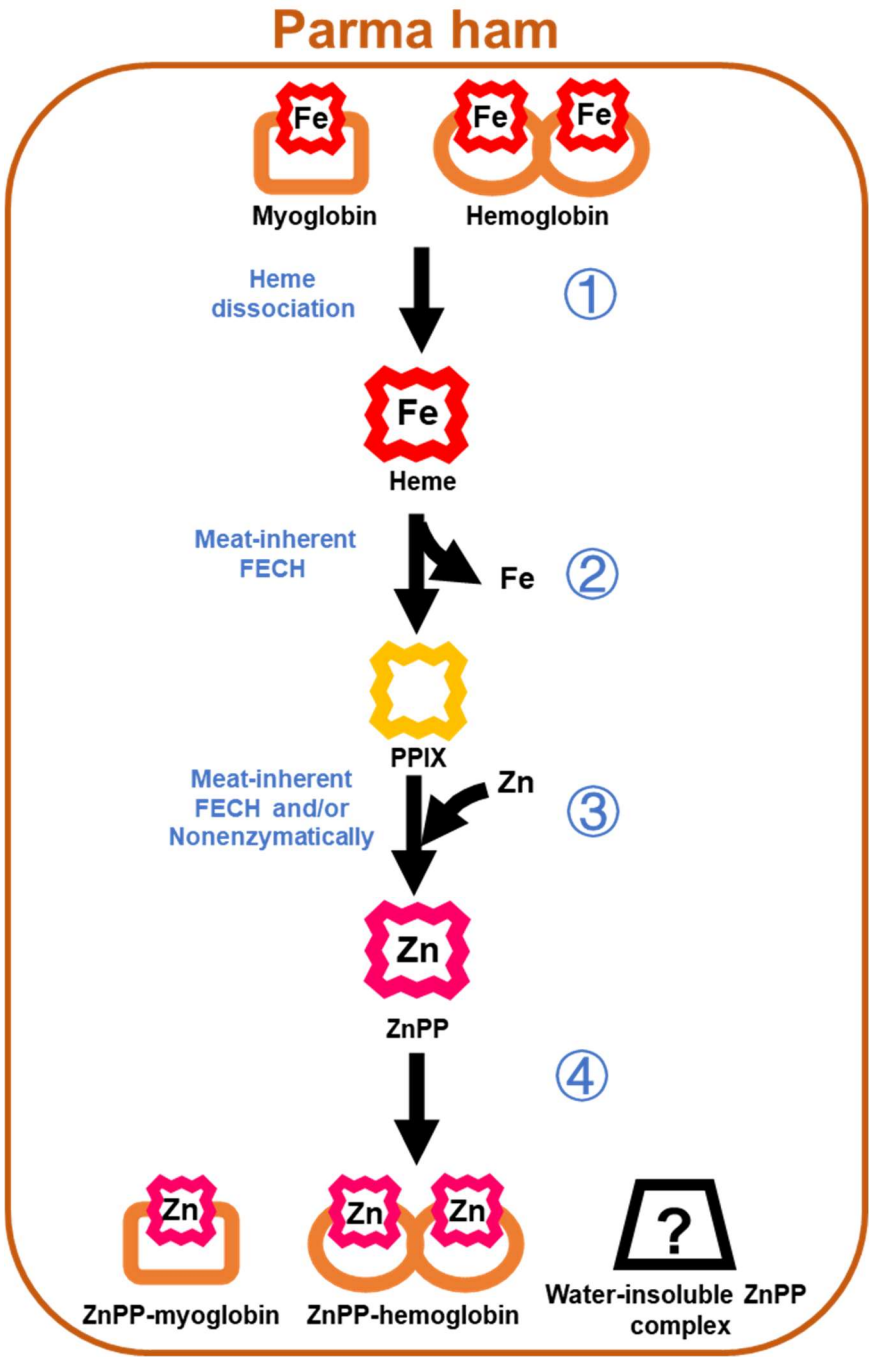

Fig. 2. The suggested formation pathway of the ZnPP and its complexes converted from the heme proteins in Parma ham

Step ①: The heme is dissociated form Hb and Mb. The heme proteins, such as Hb and Mb, were considered as the crucial substrates to provide heme as the precursor to form ZnPP in Parma ham. Since the Mb has the highest concentration in meat compared to the other heme proteins, such as Hb (Ledward, 1992), the Mb has been considered as the main substrate to provide heme to form ZnPP in Parma ham (Khozroughi *et al.*, 2019). In addition, the heme protein degradation was suggested as an important pathway for the heme dissociated from them to convert to ZnPP in Parma ham (Grossi *et al.*, 2014). However, without heme protein degradation, ZnPP could also form in the meat homogenate under anaerobic conditions (Wakamatsu *et al.*, 2019). Recently, it has been proposed that a large amount of hematin (heme) could dissociate from Hb due to the Hb scavenging system (Wakamatsu, 2022). Moreover, the previous study found that ZnPP mainly existed in Parma ham as the water-soluble complexes by binding with the entire Hb and Mb (Wang *et al.*, 2021). Therefore, the Hb as well as Mb in Parma ham may be the favorable substrate for providing heme to convert to ZnPP, and the other heme dissociation pathway rather than proteolysis may exist for ZnPP formation in Parma ham.

Step ②: The dissociated heme is converted to PPIX as the precursor to form ZnPP. According to a suggested pathway, ZnPP was formed by the insertion of zinc into PPIX, which might be formed independently rather than converted from heme (Wakamatsu *et al.*, 2007). However, recently, it was proposed that the iron-removal reaction of the free heme catalyzed by the mammalian ferrochelatase (FECH, EC 4.99.1.1) contributed to the ZnPP formation in meat (Chau *et al.*, 2010, 2011). In addition to catalyzing the insertion of ferrous ions into PPIX to form heme, *in vitro* experiment, the recombinant porcine FECH also showed the catalytic activity of the iron-removal reaction from the free heme to form PPIX (Chau *et al.*, 2010, 2011). Therefore, the iron-removal reaction of the dissociated heme to convert to PPIX catalyzed by the meat-inherent FECH was also proposed as a significant pathway for ZnPP formation in Parma ham.

Step ③: The zinc is inserted into PPIX to form ZnPP. In the final step to form ZnPP, the zinc was inserted into the PPIX, which converted from the dissociated heme. It has been reported that the mammalian FECH could insert divalent metal ions, including zinc, into porphyrins *in vitro* (Chau *et al.*, 2010). Also, the recombinant porcine FECH showed the catalytic activity for inserting zinc into PPIX to form ZnPP *in vitro* experiment (Chau

et al., 2010). However, as a long maturation time is characteristic of Parma ham production, the contribution of this enzymatic reaction to form ZnPP in the later stage of the Parma ham maturation was proposed to be very low (Becker *et al.*, 2012). In addition, it was found that zinc could directly insert into PPIX to form ZnPP without FECH catalyzation *in vitro* experiment (Becker *et al.*, 2012). Therefore, the zinc inserted into PPIX, which was catalyzed by the meat-inherent FECH and/or non-enzymatically, was proposed as the final step for ZnPP formation in Parma ham.

Step ④: The formed ZnPP is converted to the water-soluble and the water-insoluble complexes. In Parma ham, ZnPP was found to exist in two states: mainly the water-soluble ZnPP complex and patchily the water-insoluble ZnPP complex (王, 2020). Since the ZnPP itself is hydrophobic and cannot be dissolved in an aqueous medium (Wakamatsu, 2022), the water-insoluble ZnPP complex in Parma ham may exist as the ZnPP aggregation. In addition, some water-insoluble substrates in Parma ham may bind with ZnPP and exist as the water-insoluble ZnPP complex (王, 2020). On the other hand, the water-soluble ZnPP part was observed as the main states of ZnPP existed in Parma ham, which accounted for 40-60% of the total ZnPP (王, 2020). The existence of the water-soluble ZnPP complexes in Parma ham was identified as ZnPP binding with Hb and Mb as the ZnPP-Hb and ZnPP-Mb (Wang *et al.*, 2021). However, the specific formation pathway for the ZnPP-Hb and ZnPP-Mb in Parma ham remains unclear.

1.5. Objectives

The objective of the present study is to investigate the formation mechanism of ZnPP in the nitrite/nitrate-free dry-cured meat products, especially the pathway of the heme dissociate from heme proteins to convert to ZnPP (Step ① and ②) and then interact with heme proteins to form the water-soluble ZnPP complexes (Step ④). In chapter 2, the formation pathway of the water-soluble ZnPP complexes in Parma ham was investigated using a newly established ZnPP-forming experimental model. In chapter 3, the step of the heme dissociation from heme proteins on ZnPP formation was elucidated by investigating the inhibitory mechanism of nitrite on ZnPP formation, and the effect of free heme reduction on ZnPP formation was evaluated.

Chapter 2
Investigating the mechanism of the water-soluble ZnPP formation in Parma ham using a new experimental model

2.1. Introduction

Recently, it has been reported that ZnPP in Parma ham predominantly exists as the ZnPP-Hb and ZnPP-Mb (Wang *et al.*, 2021). The formation of ZnPP in dry-cured meat products is proposed to be strongly associated with Mb (Khozroughi *et al.*, 2019; Møller *et al.*, 2007) owing to its having the highest concentration in meat compared to the other heme proteins, such as Hb (Ledward, 1992). However, the content of ZnPP-Hb in Parma ham is approximately three-fold higher than that of ZnPP-Mb (Wang *et al.*, 2021). Therefore, Hb is speculated as the more favorable heme proteins in the formation of the water-soluble ZnPP in Parma ham compared with Mb.

Additionally, the heme dissociated from heme proteins was converted into ZnPP and then inserted back into the apo-form of heme proteins was suggested as the pathway for water-soluble ZnPP formation in Parma ham (Wakamatsu, 2022; Wang *et al.*, 2021). The FECH, which is proposed to be the crucial enzyme in ZnPP formation, is naturally located in the inner membrane of the mitochondria in mammalian cells (Sakaino *et al.*, 2009) and heme is abundant in heme proteins. It has been suggested that the heme dissociated from heme proteins due to the heme destabilization and then entered the mitochondria to react with FECH was related to ZnPP formation in Parma ham (Wang *et al.*, 2021), but lack of direct evidences to support this phenomenon. Furthermore, the pathway by which the formed ZnPP reacted with apo-form of heme proteins to form the water-soluble ZnPP complexes remains unclear. Therefore, the specific pathway of heme dissociated from heme proteins to form ZnPP and the interaction of ZnPP with apo-form of heme proteins need to be investigated to elucidate the formation mechanism of water-soluble ZnPP complexes in Parma ham.

Nonetheless, because producing Parma ham requires a lengthy and complicated

process, an experimental model system has been widely used to investigate the ZnPP formation in Parma ham (Khozroughi *et al.*, 2018; Wakamatsu, Okui, *et al.*, 2004b). The previous study reported that the formation of ZnPP was typically existed as two patterns in the two established experimental models, i.e. LTL model and IS model (Wakamatsu *et al.*, 2019). However, almost no water-soluble ZnPP was formed in the previous IS model with a pH value of 4.75 (王, 2020), and the degradation of heme proteins was observed during anaerobic incubation (Wakamatsu *et al.*, 2019), indicating the formation mechanism of ZnPP in the previous IS model might be different from that in Parma ham. On the other hand, the water-soluble ZnPP was observed in the previous LTL model with a pH value of 5.5 (王, 2020), which indicated that the formation pathway of ZnPP in the previous LTL model might be the same as that in Parma ham. However, the water-soluble ZnPP formation amount of the previous LTL model was very low (data not shown). In addition, to investigate the formation mechanism of water-soluble ZnPP in Parma ham using the experimental model, it is also necessary to confirm whether the water-soluble ZnPP complexes existed in the same form in both. Since the water-soluble ZnPP formation amount in the previous LTL model was not sufficient for studying its formation mechanism in Parma ham and the existing form of the water-soluble ZnPP complex in the previous LTL model remains unclear. Therefore, based on the previous LTL model, it needs to establish a new experimental model, which could produce ample amount of the same water-soluble ZnPP as Parma ham.

In this chapter, the formation pathway of the water-soluble ZnPP in Parma ham was investigated using a newly established experimental model, which could produce plenty of water-soluble ZnPP. The water-soluble ZnPP complexes formed in the new experimental model were first verified whether they were the same as those in Parma ham using HPLC, urea-PAGE, and western blotting analysis. To elucidate the formation pathway of ZnPP from the heme proteins, the exogenous Hb or Mb was added to the new experimental model, and the differences in the ZnPP formation, iron-release reaction, and the protein stability were evaluated. Finally, after the heme dissociated from heme proteins to form ZnPP and simultaneously produced the apo-form of heme proteins, the formation of the water-soluble ZnPP complexes was investigated by binding ZnPP with the apo-form of heme proteins.

2.2. Materials and methods

2.2.1. Chemical reagents

ZnPP and porcine Hb were purchased from Sigma Aldrich (Saint Louis, USA). Horse Mb was purchased from Nacalai Tesque Inc. (Kyoto, Japan). 1,10-phenanthroline, penicillin G potassium, streptomycin sulfate, and gentamicin sulfate were purchased from Fujifilm Wako Pure Chemical Corp. (Osaka, Japan).

2.2.2. Meat materials

Pork loins were obtained from three different common domestic crossbred pork cuts purchased from a local market (Hokkaido, Japan). After removing visible fat and connective tissue, each *Longissimus thoracis et lumborum* (LTL) muscle and *infraspinatus* (IS) muscle sample was vacuum-packed and stored frozen (−30°C) until use. The *quadriceps femoris* (QF) muscle of the Parma ham was obtained from three different whole hams (One whole ham was purchased from Corte Buona, Parma, Italy, the other two whole hams were purchased from Disossatura Prosciutti, Parma, Italy), after removing visible fat and connective tissue, all samples were vacuum-packed and stored frozen (−30°C) until use.

2.2.3. Parma ham water extract (PHE) preparation

After thawing, 20% Parma ham QF muscle (w/v) in ultrapure water was homogenized at 10,000 rpm in an ice bath for 120 s (Cell Master CM-100, ASONE, Tokyo, Japan). Afterwards, the homogenate was centrifuged at 38,900 × g for 30 min at 4°C (Himac CS100, Hitachi Koki Co. Ltd., Tokyo, Japan), and the supernatant was filtered through a filter paper (No. 2, Toyo Roshi Kaisha, Co. Ltd., Tokyo, Japan). The filtrate obtained from Parma ham was named as PHE.

2.2.4. Apohemoglobin (apo-Hb) preparation

Apo-Hb was prepared from porcine Hb standard as previously described (Miyazaki *et al.*, 1999) with slight modifications. The porcine Hb standard (1.6 mg) was resolved into 5 ml of 20 mM Tris-HCl buffer (pH 8.2), then added dropwise for 20 min to 50 ml of cold

(−20°C) acid-acetone that contained 0.05 ml of 35% HCl while stirring. The acid-acetone solution was then kept cold (4°C) and stirred for another 10 min, then it was let to stand for 10 min. Subsequently, the precipitate in the acid-acetone solution was collected on a filter paper using suction filtration, and washed with 100 ml of cold acetone without HCl. The suction was continued for another 20 min to dry the acetone in the precipitate. Finally, the precipitate was collected and dissolved into 4 ml of 20 mM boric acid buffer (pH 5.5) containing 0.9% NaCl. The protein concentration of extracted apo-Hb was measured by a commercial BCA kit (T9300A, Takara Bio Inc., Shiga, Japan) according to the manufacturer's protocol.

2.2.5. Non-enzymatic binding reaction of apo-Hb and ZnPP standard

The interaction of apo-Hb and ZnPP was performed according to the method described by Miyazaki *et al.*, (1999) with some modifications. The extracted apo-Hb with 0.212 mg/mL final concentration in 4 mL of 20 mM boric acid buffer at pH 5.5 was gently stirred at 4°C. The 0.2 mg/mL ZnPP standard stock in dimethylformamide (DMF) buffer was immediately added dropwise into the solution to obtain a final concentration of 10 μM. The mixture was then kept cold (4°C) and stirred for at least 1 h to allow them to react. The longest reaction time without the protein aggregation or precipitation in the mixture is 20 h. Next, the urea-PAGE experiment and the observation of ZnPP binding protein bands in the gel were performed as mentioned in Section 2.2.9.

2.2.6. ZnPP-forming experimental models

Two previous ZnPP-forming experimental models were performed according to the previous study (Wakamatsu *et al.*, 2019). After thawing, LTL or IS was homogenized with ultrapure water (20%, w/w) at 10,000 rpm in an ice bath for 120 s. After adding antibiotics into the homogenate to the final concentrations of 70 μg/ml penicillin G potassium, 250 μg/ml streptomycin sulfate, and 50 μg/ml gentamicin sulfate, the pH was adjusted with HCl to 4.75 or 5.5. Subsequently, a 20 mL homogenate of each individual solution was transferred into a 50 mL sterilized conical tube. The conical tubes were then transferred into an oxygen-impermeable storage bag containing an oxygen absorbent (A–500HS, I.S.O. Inc., Yokohama, Japan) for regulating the anaerobic conditions. Finally, all storage bags were incubated under the darkness under different conditions (Table 1).

Table 1. Incubation parameters of two previous experimental models

Parameters	LTL Model	IS Model
Muscle	*longissimus thoracis et lumborum*	*infraspinatus*
Meat content	20%	
pH	5.5	4.75
Temperature	25℃	37℃
Incubation time	7 days	
Gas condition	anaerobic	
Antibiotics	penicillin G potassium (70 μg/ml) streptomicin sulfate (250 μg/ml) gentamicin sulfate (50 μg/ml)	

The new ZnPP-forming experimental model was established based on the previous LTL model described above by optimizing four incubation parameters (Table 2). After thawing, LTL muscle was homogenized with ultrapure water (20, 30, 40, 50, 60%, w/w), and added with various antibiotics described above. The pH of the homogenate was adjusted with HCl or NaOH to 4.75, 5.0, 5.5, 6.0, and 6.5, respectively. Subsequently, a 20 mL homogenate of each solution was transferred into a 50 mL sterilized conical tube and incubated in the oxygen-impermeable storage bag with an oxygen absorbent under different temperatures and incubation time under the darkness. The optimal level of each incubation parameter of the new experimental model was determined with respect to the ZnPP-forming amount.

Table 2. Optimization of new experimental model incubation parameters

Parameters	Studied range
Muscle	*longissimus thoracis et lumborum*
Meat content	20, 30, 40, 50, 60%
pH	4.75, 5.0, 5.5, 6.0, 6.5
Temperature	25, 30, 35, 40, 50°C
Incubation time	1, 4, 7, 10, 13, 16, 19 days
Gas condition	anaerobic
Antibiotics	penicillin G potassium (70 µg/ml) streptomicin sulfate (250 µg/ml) gentamicin sulfate (50 µg/ml)

To evaluate the effect of different heme sources on ZnPP formation, Hb or Mb standard was separately added to a 50 mL sterilized conical tube containing 20 mL of the LTL homogenate (50% (w/w) LTL muscle, pH 5.5, antibiotics added) with 0.005% (w/w) final concentration. Subsequently, the conical tubes were transferred into an oxygen-impermeable storage bag with an oxygen absorbent, and incubated at 35°C under the darkness for 20 days. The amount of both total and water-soluble ZnPP was monitored during anaerobic incubation as described below.

2.2.7. ZnPP fluorescence measurement

The extraction of ZnPP in the experimental model was carried out as previously reported (Wakamatsu *et al.*, 2007). After incubation, the homogenate from each conical tube was first centrifuged at 38,900 × g for 15 min at 4°C (Himac CS100, Hitachi Koki

Co. Ltd., Tokyo, Japan), and then filtered using a filter paper. Subsequently, the separated precipitate and supernatant were separately mixed with a 75% (w/w) final concentration of cold acetone, then allowed to rest on ice for 30 min under the darkness to extract the ZnPP. After filtering the extract through a filter paper, the fluorescent intensity of ZnPP was measured using a fluorescence spectrophotometer (RF–5300PC, Shimadzu Corporation, Kyoto, Japan) at 590 nm for excitation at 420 nm. The background fluorescence intensity was eliminated by subtracting the average fluorescence intensity at 570 nm and 610 nm for ZnPP measurement. The fluorescent intensity of the model supernatant was used as a metric for the quantity of water-soluble ZnPP formed, and the fluorescence intensity of model precipitate was used as a metric for the quantity of water-insoluble ZnPP formed. The quantity of total ZnPP formed was calculated as the sum of the fluorescent intensity of the water-soluble ZnPP and water-insoluble ZnPP.

2.2.8. Observation of the changes in the structural characterization of Hb and Mb during anaerobic incubation

The Hb and Mb solution was prepared by resolving the porcine Hb standard or Mb standard into 20 mM sodium phosphate buffer (pH 5.5, containing 0.9% NaCl) with a final concentration of 1 mg/mL. The prepared Hb or Mb solution (1.5 mL) was separately transferred into a 2 mL sterilized microtube. Each solution was ventilated with nitrogen gas for at least 2 min to purge the oxygen and incubated anaerobically at 35°C under the darkness for 3 days.

Before and after incubation, the solution from Hb or Mb was centrifuged at 20,000 × g for 15 min at 4°C (Himac CT15RE, Hitachi Koki Co. Ltd., Tokyo, Japan). After filtering the extract through a filter paper, the UV-vis spectra scanning of the supernatant was performed in the range of 350 nm to 700 nm at 1 nm intervals using an UV-vis spectrophotometer (UV–1800, Shimadzu Corporation, Kyoto, Japan).

The unfolding of Hb or Mb globin proteins was observed by measuring the tryptophan (Trp) fluorescence spectrum using a fluorescence spectrophotometer (RF–5300PC, Shimadzu Corporation, Kyoto, Japan). Before and after incubation, 1 mL of Hb or Mb was applied for the fluorescence spectral analysis at the excitation wavelength of 280 nm.

2.2.9. Urea-polyacrylamide gel electrophoresis (urea-PAGE)

The ZnPP-binding proteins in the PHE and the new experimental model were separated with urea-PAGE, as described by Wang *et al.* (2021). The hand-cast gel was prepared using a 4.5% stacking gel (4.5% acrylamide including 4 M urea) and a 10% separating gel (10% acrylamide including 4 M urea). The model supernatant and PHE were individually mixed 1:1 with a sample buffer (50 mM Tris-HCl (pH 6.8), 8 M urea, 2% 2-mercaptoethanol, 40% glycerol, and 0.2% Coomassie Brilliant Blue (CBB) R-250) prior to analysis. After adding the mixture to the gel, the electrophoresis was run at 5 mA for 90 min at 4°C followed by 20 mA for 120 min at 4°C. After electrophoresis, the gel was irradiated with a 420 nm purple LED light source (OSSV5111A, OptoSupply Co. Ltd., Hong Kong, China). The fluorescent image was taken with a digital camera equipped with a 600 nm bandpass filter (BPB-60, Fujifilm Corp., Tokyo, Japan).

2.2.10. Western blotting

The proteins separated with urea-PAGE were first transferred to a polyvinylidene fluoride (PVDF) membrane. Three transfer buffers were prepared: transfer buffer A (300 mM Tris, 20% (v/v) methanol), transfer buffer B (20 mM Tris, 20% (v/v) methanol), and transfer buffer C (25 mM Tris, 20% (v/v) methanol, adjusted pH to 9.5 with boric acid). The PVDF membrane was first soaked in the methanol solution for 5 min for the hydrophilic treatment, then soaked in the transfer buffer B for 2 hours at room temperature. According to the size of the gel, six pieces of filter paper were cut out with the same area. The filter paper was then soaked in the transfer buffer A, B, and C with two, three, and one pieces for 2 hours at room temperature. The semi-dry transfer system was used for the protein signal transfer (AE-6677, ATTO Corporation, Tokyo, Japan). From the positive pole in the bottom, two filter papers in A buffer, one filter paper in B buffer, the PVDF membrane, gel, and three filter papers in C buffer were stacked in order. After removing the bubbles, the protein signals were transferred to the PVDF membrane at 2 mA/cm^2 for 50 min at room temperature. Next, the membrane was blocked with 20% (v/v) EzBlock Chemi (ATTO Corporation, Tokyo, Japan) for 45 min at room temperature, then reacted with goat polyclonal anti-Mb (10,000-fold dilution, Bethyl Laboratories, Waltham, Massachusetts, USA) or rabbit polyclonal anti-Hb (7,000-fold dilution, Cloud-

Clone Corp., Katy, Texas, USA) for 14 h at 4°C. Next, horseradish peroxidase (HRP)-conjugated anti-goat IgG (15,000-fold dilution, SeraCare Life Sciences, Milford, Massachusetts, USA) or HRP-conjugated anti-rabbit IgG (20,000-fold dilution, Jackson Immuno Research Laboratories, West Grove, Pennsylvania, USA) was reacted with the membrane for 2 h at 4°C. The protein signals were visualized using a chemiluminescence reagent (Chemi-Lumi One L, Nacalai Tesque, Kyoto, Japan) and ChemiDoc XRS Plus system (BIO-RAD, Philadelphia, Pennsylvania, USA).

2.2.11. Size exclusion-high-performance liquid chromatography (SEC-HPLC)

The supernatants (200 μL) of the new experimental model on day 0 and day 20 in the incubation period and the PHE (200 μL) were first filtered through a 0.45 μm cellulose syringe-filter (Minisart RC4, Sartorius Stedim Lab Ltd, Stonehouse, UK), the clear supernatant of each mixture was mixed with an equal volume of a mobile phase consisting 20 mM phosphoric acid buffer (pH 5.5) and 0.9% (w/w) NaCl. After added each individual mixture (10 μL) to a G3000SW column (7.5φ × 600 mm, Tosoh Corporation, Tokyo, Japan) with a flow rate of 0.5 ml/min, ZnPP was detected at 590 nm for excitation at 420 nm. The MW-HPLC marker (Oriental Yeast Co., ltd., Tokyo, Japan) was used to establish the calibration curve by detecting the absorbance of each protein at 280 nm and their retention time. The molecular weight of each fraction in the new experimental model supernatant and PHE was calculated according to the calibration curve.

2.2.12. Non-heme iron content determination

During anaerobic incubation, the non-heme iron content in the experimental model was measured according to the method described by Ahn *et al.* (1993) with slight modifications. On each sampling day, the meat homogenate (3.5 mL) was transferred into a 15 mL sterilized conical tube and mixed with 0.3 mL of 1 M citrate-phosphate buffer (pH 5.5) and 0.2 mL of 0.5 M ascorbic acid in 1 M HCl. The mixture was then incubated at room temperature for 30 min. Next, 2 mL of 11.3% trichloroacetic acid was added, and the mixture was mixed thoroughly and centrifuged at 16,200 × g for 20 min at room temperature. After it was filtered through a filter paper, the supernatant (2 mL) was mixed with 0.45 mL of 10% ammonium acetate and 0.55 mL of 0.5 mM 1,10-phenanthroline. After 30 min incubation at room temperature, the absorbance was measured at 510 nm

against a blank (2 mL distilled water + 0.45 mL, 10% ammonium acetate + 0.55 mL 1,10-phenanthroline) using a UV-vis spectrophotometer. The ferric chloride standard (Iron Standard Stock Solution, Fujifilm Wako Pure Chemical Corp., Osaka, Japan) was used to establish the calibration curve to calculate the non-heme iron content in the samples.

2.2.13. Statistical analysis

The statistical analysis was carried out with JMP Pro software version 15.2.0 (SAS Institute Inc., Cary, North Carolina, USA). The values of the ZnPP fluorescent intensity were reported as the mean ± the standard error of the mean (SEM) of three independent repetitions. A one-way analysis of variance (ANOVA) with Tukey's multiple comparison test was performed to determine each optimum water-soluble ZnPP-forming condition in the experimental model. The differences in ZnPP formation between the previous LTL model and the new experimental model were evaluated by the Student's *t*-test. Significant effects were reported at $p < 0.05$.

2.3. Results

2.3.1. Optimization of the new experimental model

Various factors, especially the meat content, temperature, pH, and incubation time affected the formation of ZnPP in the experimental model (Wakamatsu *et al.*, 2007). Therefore, these four factors were examined and the more suitable and convenient experimental model was attempted to be established.

When the meat content was increased from 20% to 50%, a significant linear increase in both the water-soluble and water-insoluble ZnPP formation was observed, with the maximum water-soluble ZnPP in 50% meat content (Fig. 3A). The homogenizing operation became obstructed when the meat content in the mixture was over 50%. In addition, in all groups, approximately 40–60% of the total ZnPP was converted into water-soluble ZnPP.

The highest water-soluble and water-insoluble ZnPP contents were both recorded when the incubation temperature was 35°C (Fig. 3B). It was notable that a decrease in both water-soluble and water-insoluble ZnPP was recorded when higher (40 and 45°C) incubation temperatures were applied. Moreover, the changes in incubation temperature showed little effect on the conversion ratio of water-soluble ZnPP.

The highest amount of water-soluble ZnPP was produced at pH 5.5 after anaerobic incubation, while either a further increasing or decreasing pH resulted in a decreasing trend in its formation (Fig. 3C). Moreover, a lower incubation pH (4.75 and 5.0) resulted in a significantly lower water-soluble ZnPP ratio of total ZnPP, which manifested negatively in the amount of water-soluble ZnPP and positively for water-insoluble ZnPP gain. When the incubation pH was at 4.75, the water-soluble ZnPP ratio of total ZnPP was the lowest (Fig. 3C). This result was consistent with the previous IS model with the pH at 4.75, showing that almost no water-soluble ZnPP was formed after anaerobic incubation (Fig. 4). In contrast, the conversion of water-soluble ZnPP occurred at a higher ratio in the experimental model when the pH was at 6.0 or 6.5.

The duration of incubation time was able to linearly increase both the water-soluble

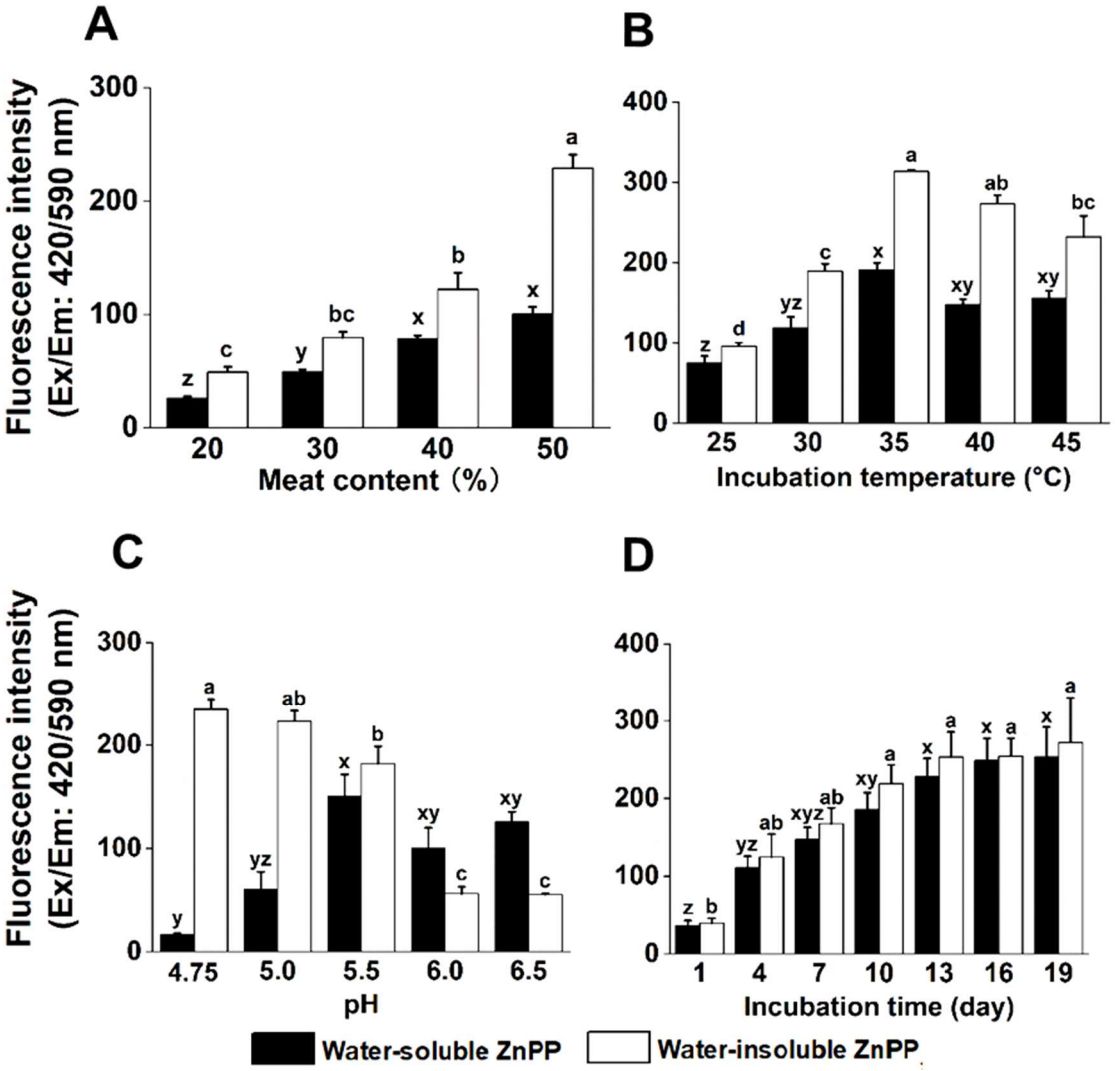

Fig. 3. Effects of meat content (A), incubation temperature (B), pH (C), and incubation time (D) on the formation of ZnPP in the experimental model

Single-factor experiments of incubation parameters, including meat content, incubation temperature, pH, and incubation time, were performed. Values are means ± SEM (n = 3). ^{xyz}: Significant differences among water-soluble ZnPP groups, ^{abcd}: Significant differences among water-insoluble ZnPP groups ($p < 0.05$).

ZnPP and water-insoluble ZnPP (Fig. 3D). However, considering the time cost and the conveniences of the experimental model, a 10-day incubation was found to be the most appropriate. Moreover, the extension of the incubation period had little effect on the conversion ratio of water-soluble ZnPP.

Overall, while determining the effect of individual factors on the water-soluble ZnPP formation, incubating 50% LTL muscle anaerobically at pH 5.5 and 35°C for 10 days was selected as the optimal condition for the new experimental model. Furthermore, ZnPP was formed entirely from the endogenous meat substrates in the model optimization experiment without any exogenous additives such as heme proteins, enzymes, or zinc atoms. The results shown in Fig. 4 revealed that, after incubating under this optimal condition, the water-soluble ZnPP amount in the new experimental model was approximately seven-fold higher than that in the previous LTL model. Similarly, the water-insoluble ZnPP content in the new experimental model was approximately four-fold higher compared to that in the previous LTL model.

2.3.2. Comparison of water-soluble ZnPP complexes between new experimental model supernatant and PHE

To confirm whether the water-soluble ZnPP complexes formed in the new experimental model are consistent with those in Parma ham, the urea-PAGE and western blotting assay were performed to identify the water-soluble ZnPP binding proteins between the new experimental model supernatant and PHE, while the HPLC analysis was performed to compare their ZnPP-related fractions.

2.3.2.1. Examination of the ZnPP-binding proteins between new experimental model supernatant and PHE using urea-PAGE and western blotting

The results in ZnPP autofluorescence image of urea-PAGE revealed that ZnPP-specific red fluorescence bands from the new experimental model supernatant had similar band patterns as those in PHE (Fig. 5 band a-b). Subsequently, these ZnPP-binding protein bands (Fig. 5 band a-c), which separated from PHE and new experimental model supernatant, were identified as ZnPP-Hb complexes (Fig. 5 anti-Hb band 1-3) using western blotting analysis with anti-Hb. This result corresponded to the previous report for Parma ham (Wang *et al.*, 2021). Additionally, the ZnPP-specific red fluorescence band d

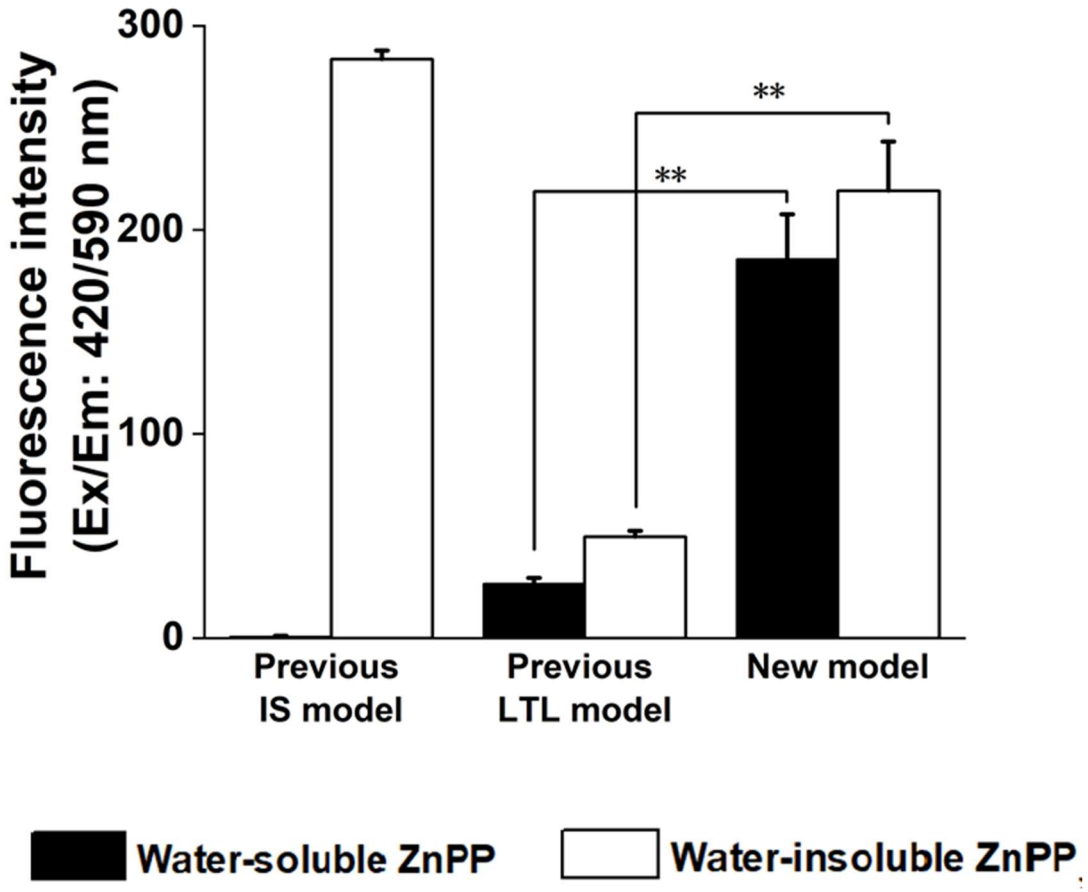

Fig. 4. The amount of ZnPP formed in previous and new experimental models

The fluorescence intensities of the water-soluble ZnPP and the water-insoluble ZnPP in the previous LTL model, the previous IS model, and the established new experimental model were measured after incubation. Values are means ± SEM (n = 3); **: $p < 0.01$.

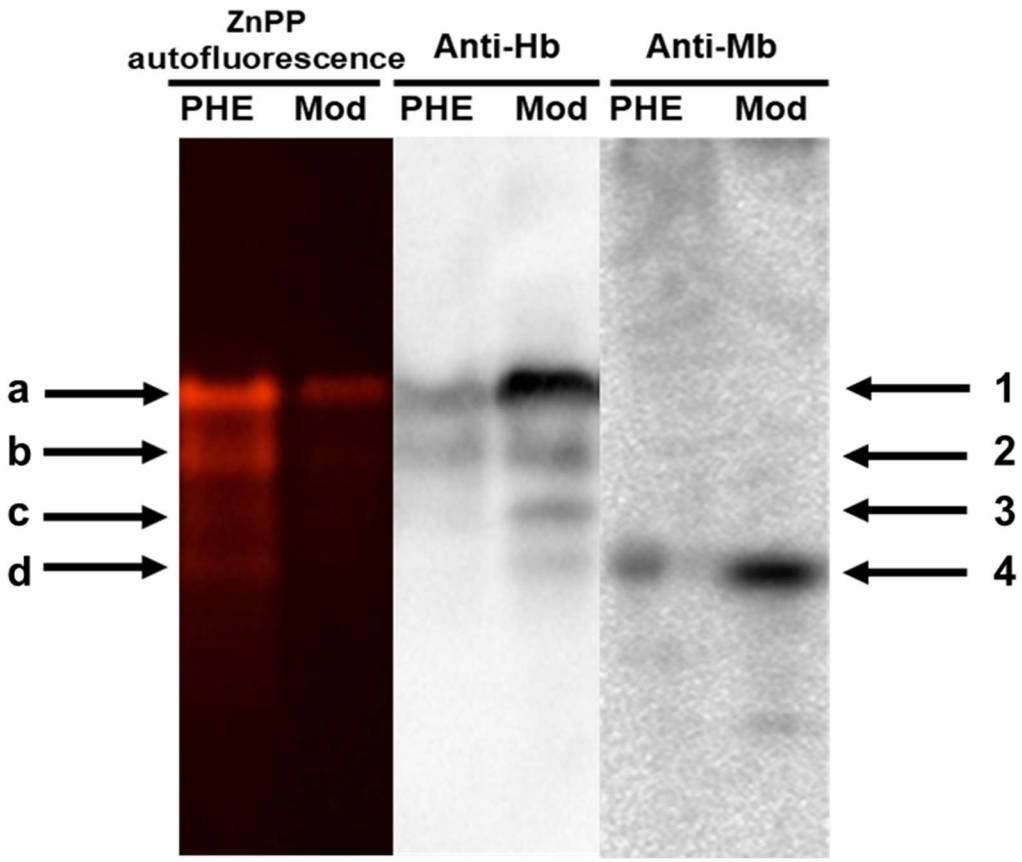

Fig. 5. ZnPP autofluorescence and western blotting images of PHE and new experimental model supernatant separated with urea-PAGE

The water-soluble ZnPP complexes in Parma ham water extract (PHE) and in the new experimental model supernatant (Mod) were separated using the urea-PAGE, the ZnPP autofluorescence detection and the western blotting analysis using anti-Hb (middle) and anti-Mb (right) antibodies were performed. a-d: ZnPP fluorescent bands; 1-4: anti-Hb or anti-Mb antibodies positive bands.

that only showed in PHE was detected as a ZnPP-Mb complex (Fig. 5 anti-Mb band 4), whereas no corresponding ZnPP-Mb band (Fig. 5 band d) was observed in the new experimental model supernatant although Mb was detected in it (Fig. 5 anti-Mb band 4). Therefore, the ZnPP-Hb complexes obtained from the new experimental model supernatant were the dominant water-soluble ZnPP complexes, similar to those in PHE.

2.3.2.2. Separation of the ZnPP-related fractions between new experimental model supernatant and PHE using SEC-HPLC

To compare the water-soluble ZnPP complexes in the new experimental model and Parma ham, the fractions with the fluorescence (Ex/Em: 420/590 nm) in the new experimental model supernatant and PHE were separated using SEC-HPLC. The fluorescence spectral analysis was next applied to verify whether these fractions separated from the new experimental model supernatant were came from the water-soluble ZnPP complexes. In the new experimental model supernatant, after 20 days incubation, there are mainly six fluorescence peaks were observed (Ex/Em: 420/590 nm), which showed an increase or no change compared with those on day 0 (Fig. 6A). After the fluorescence spectral analysis at the excitation wavelength of 420 nm, only two peak fractions with the retention time at 44.5 min and 71.5 min showed the fluorescence peaks at 590 nm (Fig. 7 arrow). Meanwhile, these two peaks in the new experimental model supernatant were also found in the PHE (Fig. 6B arrows). Next, the molecular weight of the peak fraction with the retention time at 44.5 min was calculated at about 42 kDa, whereas the molecular weight of the peak fraction with the retention time at 71.5 min was about 5 kDa. According to the previous study (王, 2020), the 42 kDa peak fraction was considered as the ZnPP-Hb dimer and the 5 kDa fraction peak was considered as the free ZnPP. Therefore, the ZnPP-Hb dimer was observed as the water-soluble ZnPP complex in both PHE and the new experimental model supernatant.

2.3.3. Supplemental effect of the exogenous Hb and Mb on ZnPP formation in the experimental model

To compare the supplemental effect of Hb and Mb on ZnPP formation, the exogenous Hb and Mb were equally added into the new experimental model before incubation. During anaerobic incubation, the differences and changes in the total ZnPP formation,

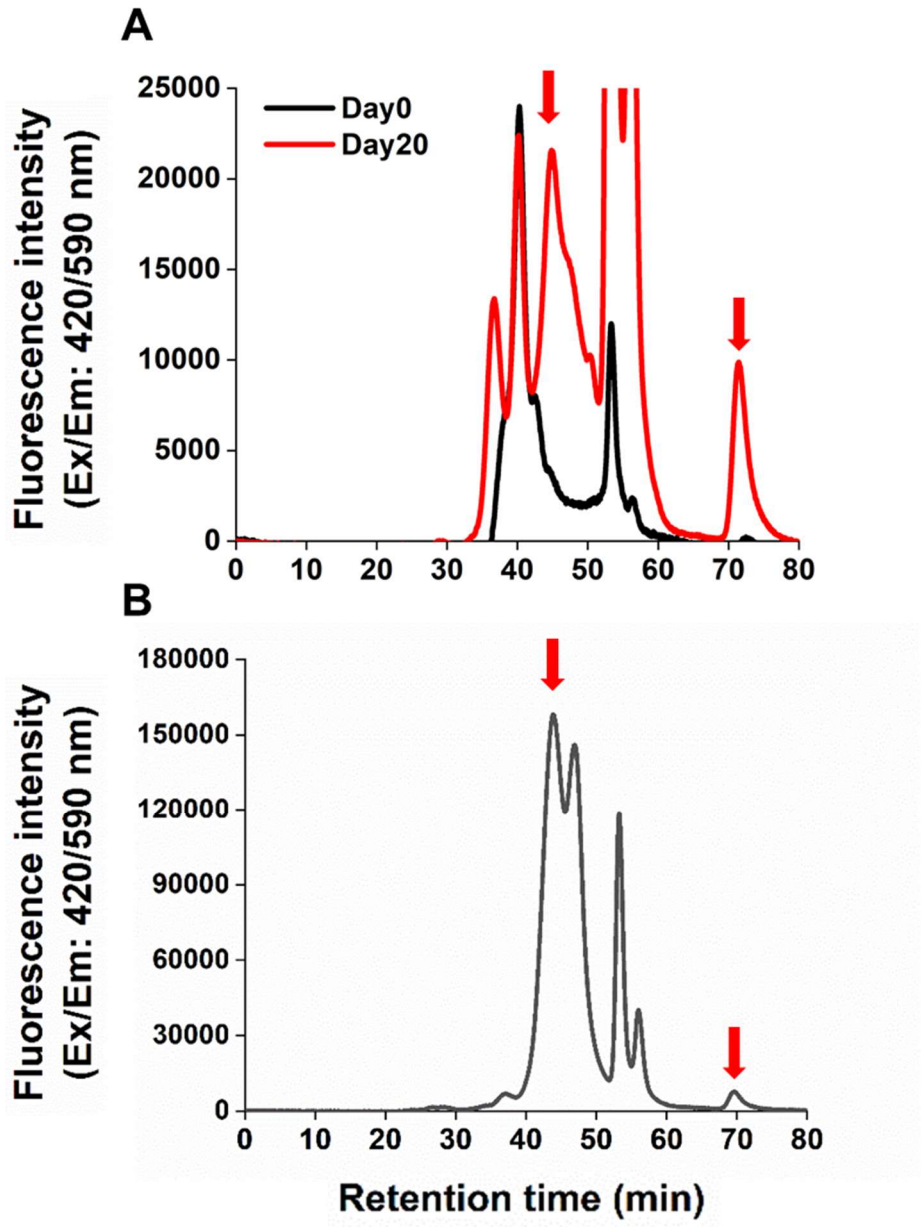

Fig. 6. SEC-HPLC fluorescence chromatograms of the new experimental model supernatant (A) and PHE (B)

The supernatants in the new experimental model on day 0 and day 20 (A) and the Parma ham extract (PHE) (B) were applied to the SEC-HPLC, and their ZnPP-related fractions were detected by measuring the fluorescence (Ex/Em: 420/590 nm). The arrows indicate the same ZnPP-related fractions in the new mode supernatant and PHE.

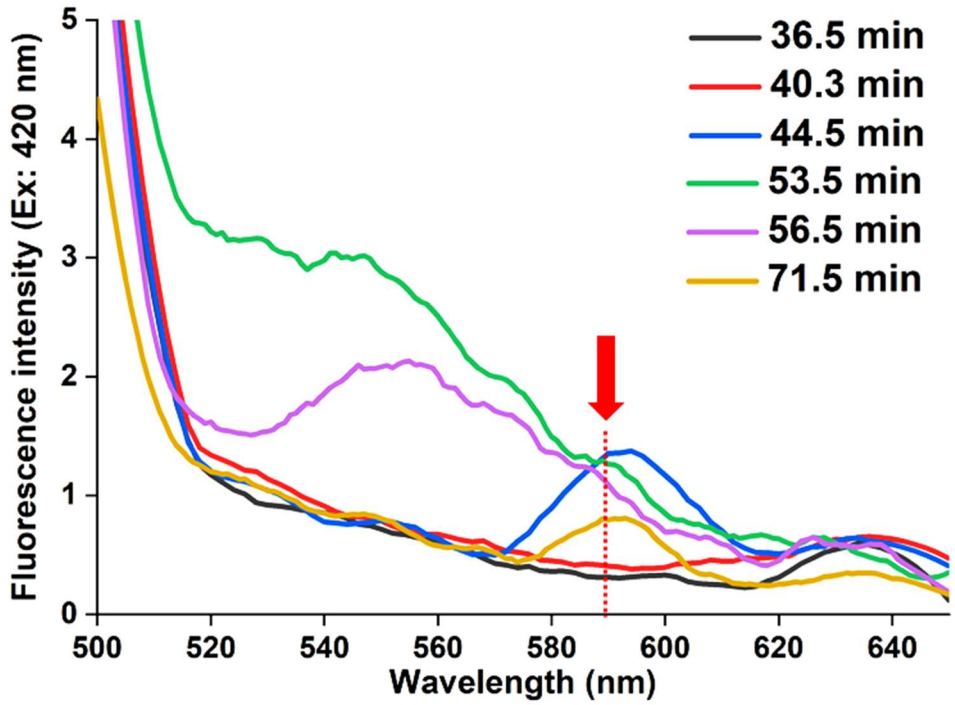

Fig. 7. Fluorescence spectrum of each peak fraction in the new experimental model supernatant separated from the SEC-HPLC

The fluorescence spectrum of each peak fraction separated from the new experimental model supernatant after 20 days incubation (Fig. 6A), were measured at the excitation wavelength of 420 nm. The arrow indicates the ZnPP characteristic fluorescence peak (590 nm).

Fig. 8. Supplemental effects of exogenous porcine Hb and Mb on total ZnPP formation (A), water-soluble ZnPP formation (B), and released non-heme iron formation (C) in new experimental model during anaerobic incubation

After the addition of the exogenous Hb or Mb (0.005%, w/w) in the new experimental model, the total ZnPP formation, the water-soluble ZnPP formation, and the released non-heme iron among Hb-added, Mb-added, and control groups were monitored during anaerobic incubation. Values are means ± SEM (n = 3). ^{abcde}: values with different letters within the same group indicate the significant differences during anaerobic incubation; ^{xy}: values with different letters within the same incubation day indicate the significant differences among groups ($P < 0.05$).

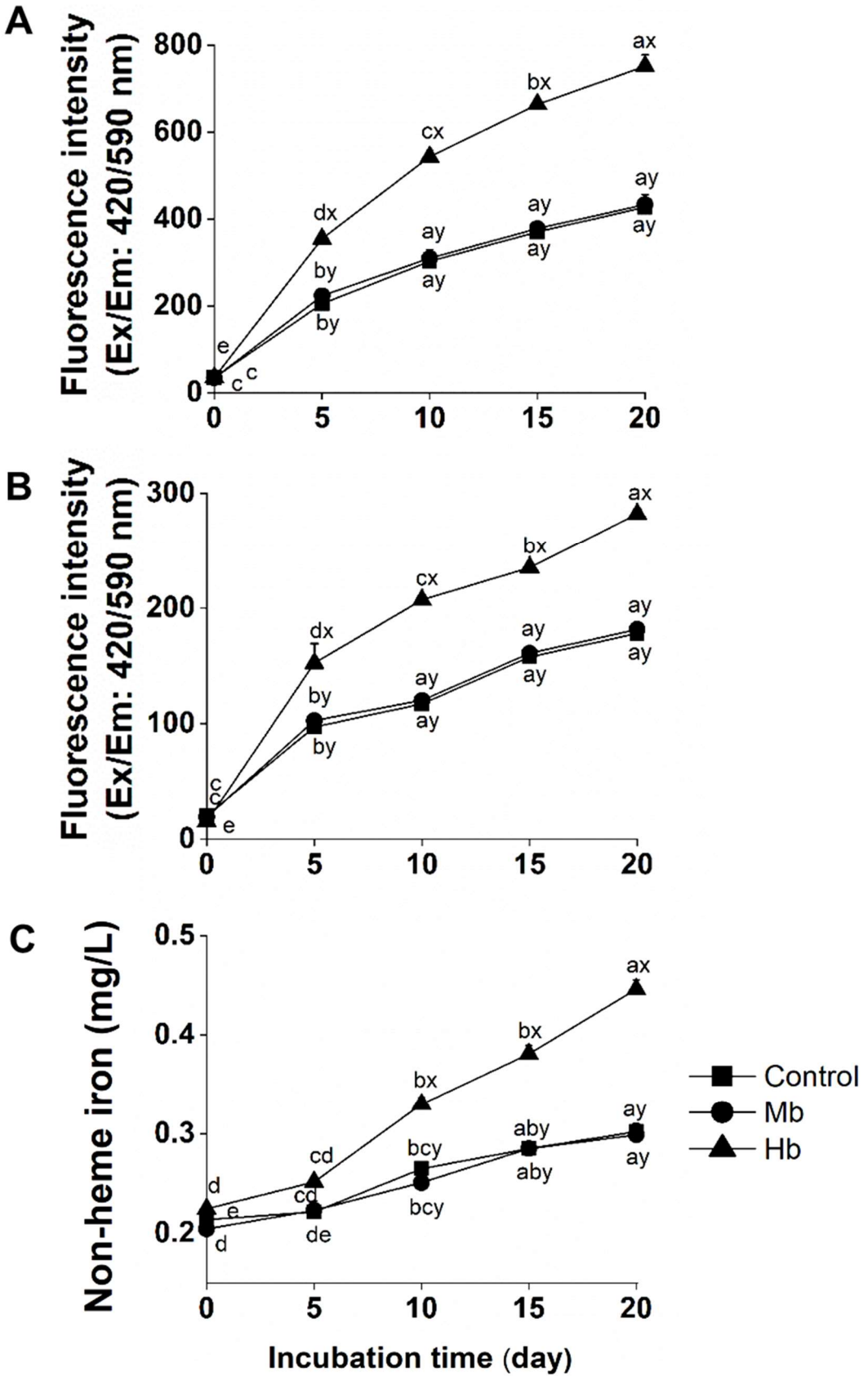
A
Fluorescence intensity (Ex/Em: 420/590 nm)
800
600
400
200
0
0
5
10
15
20
ax
bx
cx
dx
ay
by
e
c
B
Fluorescence intensity (Ex/Em: 420/590 nm)
300
200
100
0
C
Non-heme iron (mg/L)
0.5
0.4
0.3
0.2
aby
bcy
cd
de
d
Incubation time (day)
Control
Mb
Hb

water-soluble ZnPP formation, and the released non-heme iron content in different treatments were monitored. As a result, the accumulation of ZnPP during the incubation time in Hb-added, Mb-added, and control groups was confirmed (Fig. 8 A and B). The addition of Hb led to a more rapid increase in both water-soluble and total ZnPP content compared to the other groups ($p < 0.05$), whereas no significant difference among them was observed between the Mb-added and control groups. The released non-heme iron content showed a similar increase trend as ZnPP in all three groups during anaerobic incubation (Fig. 8C). The released non-heme iron content increased significantly ($p < 0.05$) in the Hb-added group compared to the other two groups. For Mb-added and control groups, no difference was observed in the increase in released non-heme iron content during anaerobic incubation ($p > 0.05$).

2.3.4. Observation of the changes of protein structural stability of Hb and Mb during anaerobic incubation

In order to evaluate the protein structural stability of Hb and Mb during anaerobic incubation, the changes in absorbance spectra and Trp fluorescence spectra of Hb and Mb were monitored as the indexes of their heme dissociation and their unfolding of globin proteins, respectively (Fig. 9 and 10).

Compared with day 0, the Soret band peak of Hb showed a notable decrease after 3 days anaerobic incubation. Similarly, the decrease of the two typical Q bands of Hb was also observed (Fig. 9A). In contrast, as for the Mb, compared with day 0, almost no change was detected in its Soret band peak and two typical Q bands (Fig. 9B) after 3 days anaerobic incubation.

Furthermore, the Trp fluorescence intensity of Hb was notably increased after 3 days anaerobic incubation (Fig. 10A). As for Mb, compared with day 0, although its Trp fluorescence intensity showed an increase trend after 3 days anaerobic incubation, the extent of the increase was much lower than that of Hb (Fig. 10B).

Therefore, compared with Mb, Hb showed an unstable heme-globin structure under anaerobic conditions.

2.3.5. Non-enzymatic binding reaction of apo-Hb and ZnPP

To investigate whether ZnPP could directly bind with apo-Hb to form the ZnPP-Hb

complex, the apo-Hb solution was first mixed with the ZnPP standard, and the ZnPP-Hb fluorescent bands were observed in urea-PAGE and compared with those in both the PHE and the new experimental model supernatant. As a result, no fluorescent band was observed in the apo-Hb lane, which was added only the apo-Hb solution. After only mixing apo-Hb solution with the ZnPP standard (ZHb lane), the ZnPP-Hb fluorescent bands were detected and showed almost the same position as those in the new experimental model supernatant (Mod lane) and PHE (Fig. 11 band 1 and 2). In addition, the band 4 (Fig. 11), which was reported as the ZnPP-Mb complex (Wang *et al.*, 2021), was only observed in PHE. Meanwhile, band 5 (Fig. 11) in both the ZnPP binding apo-Hb group (ZHb lane) and PHE was considered as the free ZnPP.

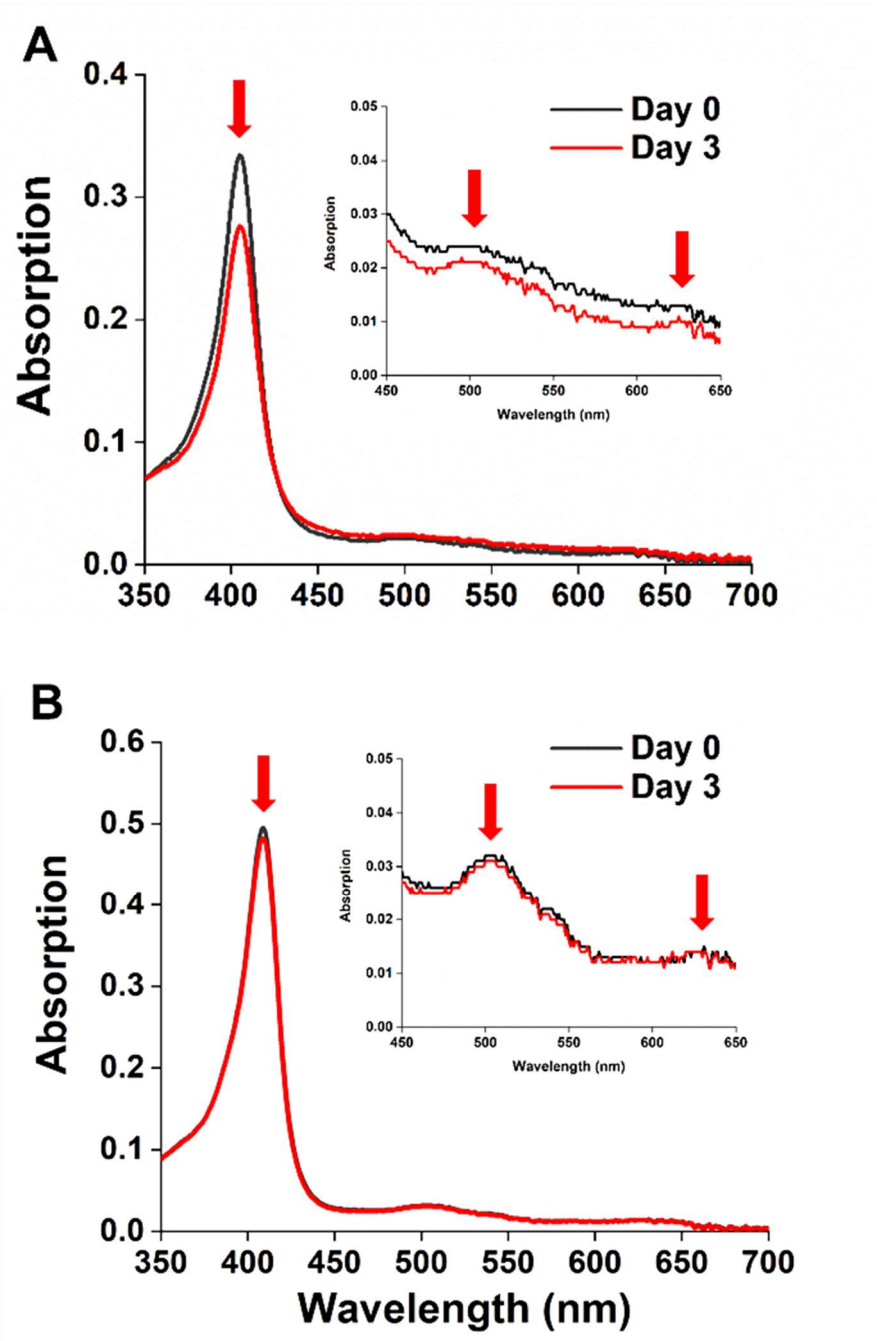

Fig. 9. UV-visible absorption spectrum of Hb (A) and Mb (B) during anaerobic incubation

The UV-visible absorption spectra changes of the Hb and Mb were observed before and after 3 days anaerobic incubation at 35°C. The inserted image shows the enlarged spectra of the specific Q bands. The arrows indicate the characteristic peaks of Hb and Mb.

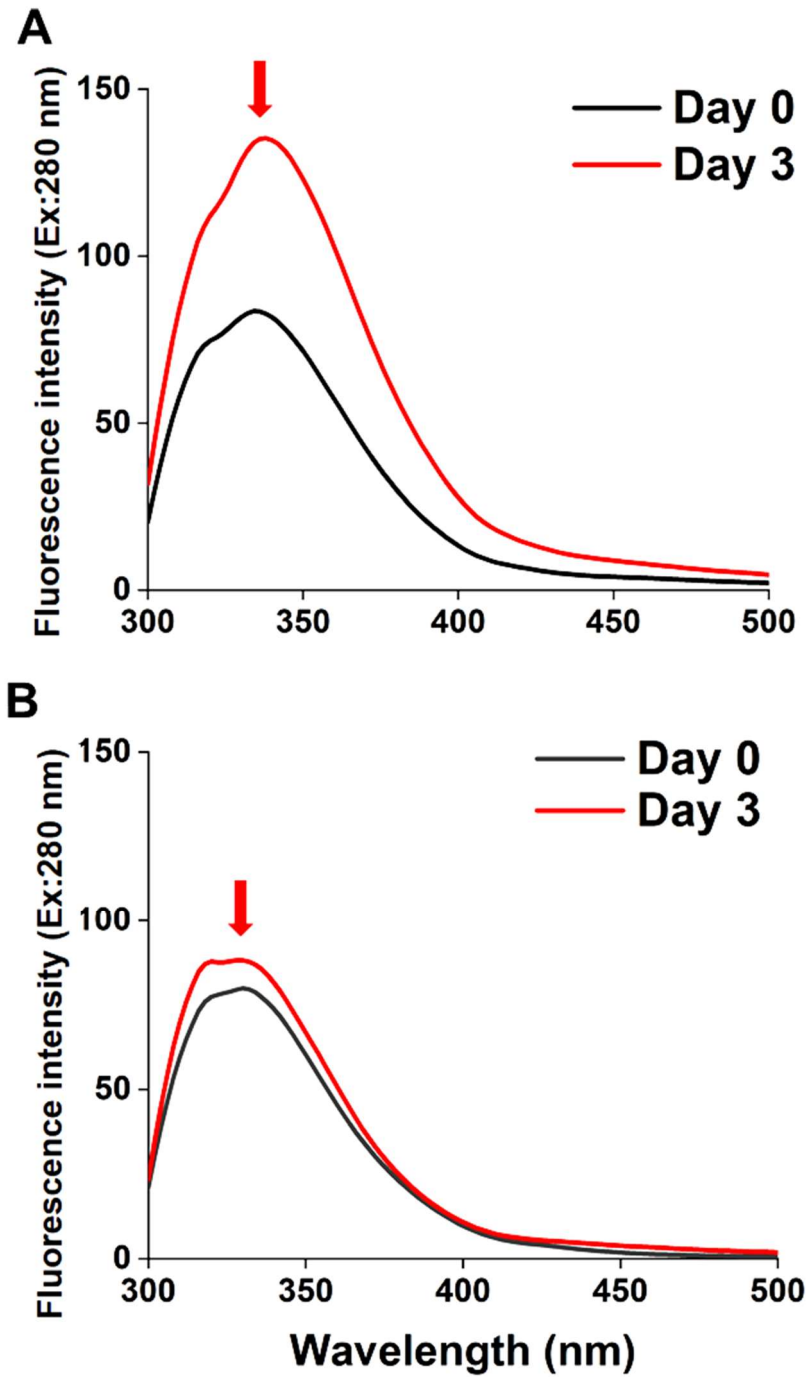

Fig. 10. Changes in the fluorescence spectrum derived from the Trp in Hb (A) and Mb (B) during anaerobic incubation

The fluorescence spectra derived from the Trp in Hb and Mb were observed at the excitation wavelength of 280 nm before and after 3 days anaerobic incubation at 35℃. The arrows indicate the Trp-derived fluorescence of Hb and Mb.

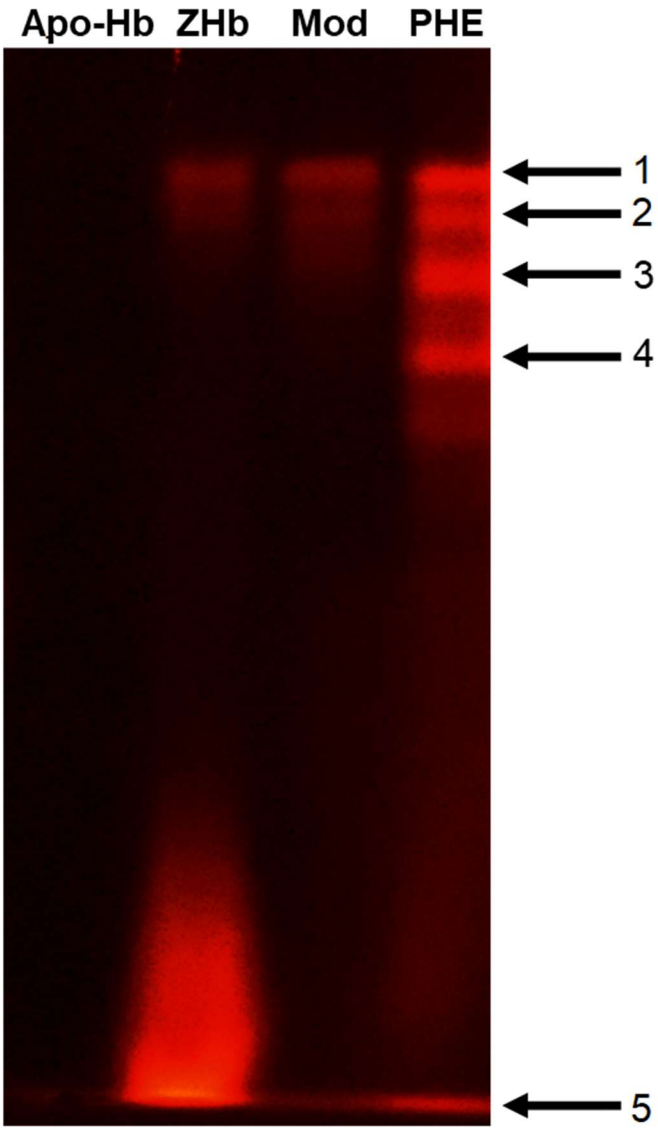

Fig. 11. Fluorescence image of apo-Hb and ZnPP standard mixture separated using urea-PAGE

The mixture prepared by mixing the apo-Hb solution with the ZnPP standard (ZHb), the apo-Hb solution (Apo-Hb), the Parma ham water extract (PHE), and the new experimental model supernatant (Mod) were applied to the urea-PAGE, and the ZnPP autofluorescence was detected. 1-5: ZnPP fluorescent bands.

2.4. Discussion

The newly established experimental model could produce seven-fold water-soluble ZnPP higher than the previous LTL model by incubating 50% porcine LTL muscle anaerobically at pH 5.5 for 20 days at 35°C (Fig. 4). The main water-soluble ZnPP complex in the new experimental model supernatant was identified as ZnPP-Hb dimer, which was almost same as that in PHE (Fig. 5 and 6). Therefore, this newly established experimental model was suitable for investigating the formation mechanism of water-soluble ZnPP in Parma ham due to its ample water-soluble ZnPP production, and the main water-soluble ZnPP complex was the same as Parma ham as ZnPP-Hb dimer.

The exogenous addition of Hb in the new experimental model promoted the formation of the total ZnPP, the water-soluble ZnPP, and the released non-heme iron under the anaerobic conditions (Fig. 8). Since the heme dissociated from heme proteins without proteolysis was considered as the significant step for ZnPP formation (Wakamatsu, 2022; Wang *et al.*, 2021), the low heme-globin binding stability of Hb (Fig. 9A and 10A) might cause a high dissociation of heme as the precursor to form ZnPP in the new experimental model. The structure of Hb is a heterotetramer consisting of two pairs of globin, and each globin binds with one heme. In the crystal structures of Hb, the Leu(F7) and Leu(FG3) in both the Hb α and β chains cannot form stable contacts with heme-7-propionate owing to the non-polar nature of leucine and the relatively large distance between the leucine side chain and the heme-7-propionate (Cai *et al.*, 2016; Hargrove *et al.*, 1994). This phenomenon resulted in a weak heme-globin binding of Hb in the new experimental model under anaerobic conditions (Fig. 9A and 10A). Thus, a large amount of heme could dissociate form the heme pocket of Hb to convert to ZnPP through the iron-removal reaction, which induced in the corresponding increase of the released non-heme iron content with ZnPP formation in the model (Fig. 8 A and C). On the other hand, it has been reported that the globin and heme moiety of Hb becomes rapidly autoxidized owing to the loss of the Hb reducing enzyme system after hemolysis (Schaer *et al.*, 2014), which could result in a large amount of heme dissociated from Hb (Hargrove *et al.*, 1994). In addition, in meat, after hemolysis, the tetrameric Hb leaks from the erythrocytes, is immediately dissociated into dimeric Hb (Schaer *et al.*, 2014), but does not further

dissociate into monomeric Hb (Kranen *et al.*, 1999). Thus, with the heme dissociated from the Hb dimer due to its weak protein structure and autoxidation rather than proteolysis, the apo-form of Hb dimer would be produced simultaneously. After the dissociated heme converted to ZnPP, the formed ZnPP might insert or interact with the apo-Hb dimer to form the ZnPP-Hb dimer, which was observed in both the new experimental model and Parma ham (Fig. 5 and 6). Therefore, Hb dimer was easy to dissociate a large amount of heme due to its unstable heme-globin binding structure, and the dissociated heme was converted to ZnPP and then insert or interact with the remaining apo-Hb dimer to form the ZnPP-Hb dimer as the main water-soluble ZnPP complex in Parma ham.

In contrast, the exogenous addition of Mb in the new experimental model showed no supplemental effect on the total ZnPP and water-soluble ZnPP formation and the released non-heme iron content (Fig. 8). Different from Hb, in the crystal structures of Mb, the heme-7-propionate is linked to nearby surface amino acids residues, such as Leu89, Ser92, His93, and His97, to form a hydrogen bonding lattice that lead to the high stability of its heme-globin binding (Fig. 9B and 10B) (Hunter *et al.*, 1997; Ledward, 1992). This stable crystal structure of Mb makes less exposure of heme from its heme pocket, resulting in less heme can dissociate from Mb to convert to ZnPP through the iron-removal reaction. Thus, in the new experimental model, no increase of both ZnPP and the released non-heme iron content were observed in the exogenous Mb-added group compared with those in the control group during anaerobic incubation (Fig. 8 A and C). In addition, although the autoxidation of Mb is almost 11-fold faster compared to that of Hb in acidic conditions (Cai *et al.*, 2016), metMb can be reduced in meat *via* enzymatic, non-enzymatic, and electron-transport pathways (Ramanathan *et al.*, 2020). Thus, less heme was thought to dissociated from Mb due to its autoxidation. Since the heme was hard to dissociate from Mb, the production of the apo-Mb might be negligible, induced in almost no ZnPP-Mb was observed in the new experimental model (Fig. 5). Similarly, it has been reported that the amount of ZnPP-Mb complexes was only a quarter of the total water-soluble ZnPP complexes in Parma ham (Wang *et al.*, 2021). Therefore, due to the stable heme-globin binding structure and the low autoxidation of Mb, less heme could dissociate form its heme pocket to convert to ZnPP, further resulting in the less ZnPP-Mb formation in Parma ham.

Additionally, after only mixing the apo-Hb solution with ZnPP, ZnPP-Hb fluorescent bands were observed, which showed almost the same position as those in PHE (Fig. 11). Since a large amount of heme could dissociate from Hb dimer due to its unstable heme-globin structure as mentioned above, the apo-Hb dimer might produce simultaneously. To form the ZnPP-Hb dimer complex, the ZnPP needs to bind with the apo-Hb dimer. Previous research on the binding reaction of cationic porphyrin to plasma proteins indicated that four kinds of amino acids, Val116, Tyr138, Lys190, and Phe149, have an equal effect on the embedment of heme and cationic porphyrins into the binding pocket of human serum albumin (Gyulkhandanyan *et al.*, 2013). Moreover, since the apo-Hb can bind to hydrophobic molecules in its vacant hydrophobic heme-binding pocket, ZnPP as the hydrophobic substance might be able to directly insert into the heme pocket of apo-Hb (Wakamatsu, 2022). Similarly, the binding reaction of apo-Hb and ZnPP was found to occur in the absence of any enzyme in this chapter (Fig. 11). Since the formed ZnPP-Hb complex showed almost same as that in Parma ham and the new experimental model, this formed ZnPP-Hb was speculated as the ZnPP-Hb dimer (Fig. 11). Therefore, after heme dissociated form Hb dimer to converted to ZnPP, the ZnPP could further non-enzymatically inserted into the simultaneously produced apo-Hb dimer to form the ZnPP-Hb dimer in Parma ham. As for ZnPP-Mb complex in Parma ham, this non-enzymatic binding may be able to occur, but more study is need to provide direct evidence.

In summary, the newly established experimental model was suitable for investigating the formation mechanism of water-soluble ZnPP in Parma ham because it could produce plenty amount of the same water-soluble ZnPP complex as Parma ham. Using this new experimental model, the feasible formation pathway of ZnPP-Hb and ZnPP-Mb in Parma ham was revealed. Due to the unstable heme-globin binding and high autoxidation of Hb dimer, heme is easily dissociated from its heme pocket and the apo-Hb dimer is simultaneously produced. The heme dissociated from Hb dimer is converted to ZnPP and then non-enzymatically inserted into the apo-Hb dimer to form a large amount of ZnPP-Hb dimer in Parma ham. Regarding the ZnPP-Mb, its formation pathway is speculated to be similar to that of ZnPP-Hb, but the stable heme-globin binding and low autoxidation of Mb may result in a very slow heme dissociation from its heme pocket, further resulting in the less formation of ZnPP-Mb in Parma ham.

Chapter 3

Investigating the inhibitory mechanism of nitrite on ZnPP formation in dry-cured meat products

3.1. Introduction

Nitrite or/and nitrate, which are added to common cured meat products, were found to inhibit the formation of ZnPP (Wakamatsu *et al.*, 2010). This phenomenon was proposed as the NO, which derived from nitrite, can inactivate the mammalian FECH (Wakamatsu *et al.*, 2010). In addition to catalyzing the insertion of ferrous ions into PPIX to form heme in living body, the mammalian FECH has been reported to contribute to ZnPP formation in meat because it had the ability to catalyze the iron-removal reaction of free heme to form PPIX and catalyze the insertion of zinc into PPIX to form ZnPP (Chau *et al.*, 2010, 2011). Meanwhile, the mammalian FECH contains a [2Fe-2S] cluster (Sellers *et al.*, 1996), but this cluster is oxygen- and temperature-labile and sensitive to NO (Furukawa *et al.*, 1995; Weerth *et al.*, 2021). Therefore, the NO derived from nitrite is thought to inhibit ZnPP formation in meat by degrading the [2Fe–2S] cluster of mammalian FECH, further suppressing its catalytic activity of iron-removal and zinc insertion.

On the other hand, the heme dissociated from heme proteins was proposed as a significant step for ZnPP formation in meat (Wakamatsu, 2022; Wang *et al.*, 2021), which has been also supported in Chapter 2. While, the heme in heme proteins can bind with many ligands, some of them strongly bind to the heme iron and stabilize both the heme structure and the heme protein structure. For instance, NO could interact with either the ferrous (Fe^{2+}) heme or the ferric (Fe^{3+}) hematin in heme proteins to form the highly stable nitrosyl heme proteins (Radi, 1996). Thus, besides suppressing the catalytic activity of iron-removal and zinc insertion of mammalian FECH by degrading its [2Fe–2S] cluster, it is possible that NO derived from nitrite can inhibit ZnPP formation by limiting either the heme or the hematin dissociation from the heme proteins in the nitrified cured meat products. Similar to NO, the carbon monoxide (CO) can bind to the ferrous heme of heme proteins to form the structural stable carboxy heme proteins (Xu *et al.*, 2016). However, CO does not causes disassembly of the FECH [2Fe-2S] cluster in meat, and does not

inhibit the insertion of iron into PPIX to form heme catalyzed by FECH (Sellers *et al.*, 1996). Therefore, it may be suitable to use CO as the comparison to elucidate whether nitrite can inhibit ZnPP formation by suppressing the heme dissociation from heme proteins in nitrified cured meat products.

Moreover, it has been reported that ZnPP in Parma ham was mainly converted from the heme dissociated from Hb (Wakamatsu, 2022; Wang *et al.*, 2021), whereas this phenomenon was proposed to be induced by the easily oxidizable properties of Hb to methemoglobin (mHb) (Hargrove *et al.*, 1994; Schaer *et al.*, 2014). The autoxidation of Hb to mHb may result in a large amount of hematin dissociated from it due to the Hb scavenging system (Ascenzi *et al.*, 2005). On the other hand, the heme-globin binding of mHb was unstable than Hb (Hargrove *et al.*, 1994), which may lead to the hematin dissociated from mHb as the precursor to form ZnPP. In contrast, the azide ion can bind to the hematin (Fe^{3+}) of the mHb to form the structural stable azide-mHb (N_3mHb) (Alben & Fager, 1972), and the addition of sodium azide as a preservative in the ZnPP-forming experimental model suppressed ZnPP formation (Wakamatsu, Okui, *et al.*, 2004). Since NO could not only bind with heme (Fe^{2+}) but also hematin (Fe^{3+}) of heme proteins to form the stable nitrosyl heme proteins. Therefore, the azide ion may be suitable as the comparison to elucidate whether nitrite could inhibit ZnPP formation by suppressing the hematin dissociation from mHb in nitrified cured meat products.

Additionally, some reductants, such as dihydronicotinamide adenine dinucleotide (NADH), dithiothreitol, and ascorbic acid, has been reported to be essential for the iron-removal reaction of hematin to form ZnPP under anaerobic conditions (Chau *et al.*, 2011; Taketani *et al.*, 2007). Also, the oxidation with an oxidation-reduction potential (ORP) value over 100 mV significantly inhibited ZnPP formation in meat homogenate (Wakamatsu *et al.*, 2010). These results indicated that the heme reduction may be significant for ZnPP formation in meat. However, with the ORP reduced to -100 mV, a notable decrease of ZnPP was also observed (Wakamatsu *et al.*, 2010). Therefore, although the heme reduction is important for the formation of ZnPP, it may have the upper limitation, and more study is needed to investigate this phenomenon.

This chapter aimed to clarify the heme dissociation from the heme proteins in the formation mechanism of ZnPP in meat. For this purpose, the inhibitory pathway of nitrite

on ZnPP formation was investigated, and CO and sodium azide are used as comparisons. Since the Hb was proposed as the main substrate to dissociate heme to form ZnPP (Wakamatsu, 2022; Wang *et al.*, 2021), which has been also supported in Chapter 2. Thus, various Hb derivatives were added into the new experimental model established in Chapter 2, and the supplemental effect on ZnPP formation, the protein stability, and the heme release amount of each Hb derivative under anaerobic incubation were evaluated. Meanwhile, the effect of the heme reduction on ZnPP formation was evaluated.

3.2. Material and methods

3.2.1. Chemical reagents

Sodium azide and sodium nitrite were purchased from Kanto Chemicals Co. Inc. (Tokyo, Japan). 1-methylimidazole (1MI) was purchased from Nacalai Tesque Inc. (Kyoto, Japan). Pure CO gas (99%) was purchased from Taiyo Nippon Sanso JFP Corp. (Kanagawa, Japan).

3.2.2. Raw materials

Pork loins were obtained from three different common domestic crossbred pork cuts purchased from a local market (Hokkaido, Japan). After removing visible fat and connective tissue, each LTL muscle sample was vacuum-packed and stored frozen (−30°C) until use. Porcine liver was purchased from a local supermarket (Hokkaido, Japan). The liver was packaged (10 g portions) in vacuum bags and stored at −30°C until use.

3.2.3. Preparation of OxyHb, NOHb, COHb, and N_3mHb derivatives

To obtain the oxyhemoglobin (OxyHb) solution, porcine Hb standard was resolved into 20 mM sodium phosphate buffer (pH 5.5, containing 0.9% NaCl) with a final concentration of 0.5 mg/mL, and then 40 mg of sodium hydrosulfite was added to 10 mL of the mixture. The mixture was stirred for at least 10 min at room temperature (25°C). Subsequently, 10 mL of the mixture was dialyzed against 1L of the pure water for 2 hours at 4°C to remove excess sodium hydrosulfite.

The nitrosyl Hb (NOHb) solution was prepared following the method described by Ma *et al.* (2022) with some modifications. The entire process of preparing NOHb was carried out under the darkness wherever possible. The porcine Hb standard was resolved into 20 mM sodium phosphate buffer (pH 7.5, containing 0.9% NaCl) with a final concentration of 0.5 mg/mL, then sodium nitrite and sodium ascorbate were added with the final concentration of 8.7 μM and 10 μM, respectively. The pH of the mixture was adjusted to 5.5 with 1 M ascorbic acid. Subsequently, the mixture was ventilated with nitrogen gas for at least 2 min to purge the oxygen and placed for at least 30 min at room temperature

to obtain the NOHb solution. Finally, 10 mL of the NOHb solution was dialyzed against 1L pure water for 2 hours at 4°C to remove excess sodium nitrite and sodium ascorbate.

The entire process of preparing carboxyhemoglobin (COHb) was carried out under the darkness wherever possible. About twice volume of pure CO gas was slowly injected to the 0.5 mg/mL OxyHb solution with vigorous stirring and placed for at least 15 min at room temperature to obtain the COHb solution. Subsequently, the COHb solution was ventilated with nitrogen gas for at least 2 min to purge the excess dissolved CO.

To obtain the N_3mHb solution, sodium azide was added to 0.5 mg/mL of the porcine Hb standard solution (20 mM sodium phosphate buffer, pH 5.5, containing 0.9% NaCl) with 0.23 μM of the final concentration. The mixture was stirred for at least 10 min at room temperature to obtain the N_3mHb solution. Subsequently, 10 mL of the mixture was dialyzed against 1L pure water for 2 hours at 4°C to remove excess sodium azide.

3.2.4. Preparation of crude pork liver FECH

The process of FECH extraction carried out was based on the procedure described by Abril *et al.* (2021) with some modifications. First, about 4 g of the porcine liver was homogenized with 100 mL of the extraction buffer at 10,000 rpm in an ice bath for 1 min. The extraction buffer contained 50 mM Tris-HCl (pH 8.0), 20% (w/v) glycerol, 0.8% (w/v) KCl, and 1% (w/v) Triton X-100. The protease inhibitor cocktail (Nacalai Tesque Inc., Kyoto, Japan) was then added into the mixture to avoid FECH degradation. Subsequently, an ultra-sound assistance (Bioruptor UCD-200T, Cosmo Bio Co., Ltd, Tokyo, Japan) using the middle power available (160 W) at a frequency of 20 kHz was applied for 1 min (10 s power on, 10 s power off) to help to extract FECH. To separate the enzyme fraction, the mixture was centrifuged at 12,500 rpm for 10 min at 4°C (Himac CS100, Hitachi Koki Co. Ltd., Tokyo, Japan). The supernatant was filtered through a filter paper (No. 2, Toyo Roshi Kaisha, Co. Ltd., Tokyo, Japan) to be used as the crude FECH extract. The existence of the FECH extracted from the porcine liver was confirmed (Fig. 12) using SDS-PAGE and western blotting as shown in Section 3.2.14.

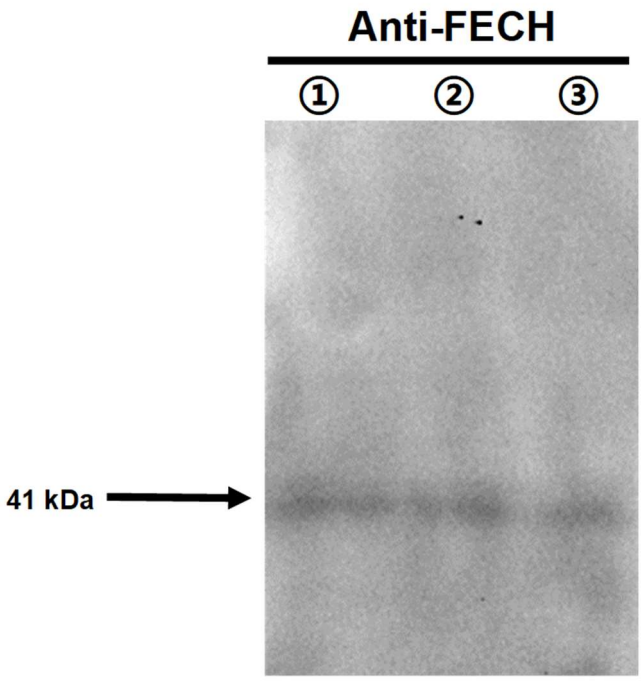

Fig. 12. Western blotting image of the crude FECH extracted from porcine liver

After the extraction of the crude FECH from the porcine liver, the mixture was applied to the SDS-PAGE, and the western blotting analysis was performed using the anti-FECH antibody. ①②③: three individuals of the crude FECH extracts. The arrow indicates the anti-FECH antibody positive band.

3.2.5. Preparation of hemin-1MI solution

The hemin standard was added into the 20 mM phosphate buffer (pH 7.5) to a final concentration of 2.5 mM. Next, the 1MI was added into the mixture with 10 mM final concentration to help hemin dissolve in the aqueous solution. After mixing for at least 10 min at room temperature, the mixture was stored at 4°C under the darkness as the stock solution.

3.2.6. Observation of the changes in the structural characterization of various Hb derivatives during anaerobic incubation

The OxyHb, COHb, NOHb, or N_3mHb solution (1.5 mL) was separately transferred into a 2 mL sterilized microtube. Each solution was ventilated with nitrogen gas for at

least 2 min to purge the oxygen and then transferred into an oxygen-impermeable storage bag containing an oxygen absorbent for regulating the anaerobic conditions. Finally, all storage bags were incubated at 35°C under the darkness for 20 days.

On each sampling day during anaerobic incubation, the solution from each Hb derivative was centrifuged at 20,000 × g for 15 min at 4°C (Himac CT15RE, Hitachi Koki Co. Ltd., Tokyo, Japan). After filtering the extract through a filter paper, the UV-vis spectra scanning of the supernatant was performed in the range of 350 nm to 700 nm at 1 nm intervals using an UV-vis spectrophotometer (UV–1800, Shimadzu Corporation, Kyoto, Japan).

The unfolding of each Hb derivative globin protein was monitored by measuring the Trp fluorescence spectrum during anaerobic incubation using a fluorescence spectrophotometer (RF–5300PC, Shimadzu Corporation, Kyoto, Japan). On each sampling day, 1 mL of each Hb derivative solution was applied for the fluorescence spectral analysis at the excitation wavelength of 280 nm.

3.2.7. ZnPP/PPIX-forming experimental models

The new ZnPP-forming experimental model was established based on the optimum conditions obtained from Chapter 2. Briefly, a total 10 mL homogenate containing 50% (w/w) porcine LTL muscle was anaerobically incubated at pH 5.5 and 35°C under the darkness for 20 days. The detail operation steps were described in Chapter 2 Section 2.2.6. For the investigation of PPIX formation in the new experimental model, 0.5 mM EDTA (final concentration) was added to suppress its conversion to ZnPP. To evaluate the supplemental effect of different Hb derivatives on ZnPP formation, each OxyHb, COHb, NOHb, and N_3mHb solution was separately added to a 15 mL sterilized conical tube containing 10 mL of the LTL homogenate (50% (w/w) LTL muscle, pH 5.5, antibiotics added) with 0.005% (w/w) final concentration. Additionally, the effect of the sodium nitrite, sodium azide, and CO on ZnPP formation in the new experimental model was evaluated respectively. For the sodium nitrite treatment, the sodium nitrite was added to a 15 mL sterilized conical tube containing 10 mL of the LTL homogenate (50% (w/w) LTL muscle, pH 5.5, antibiotics added) at a final concentration range of 0-80 μM, and then incubated for 10 days. For the sodium azide treatment, the sodium azide was added

to the LTL homogenate at a final concentration range of 0-16 mM. About twice volume of pure CO gas was injected into the LTL homogenate for the CO treatment. The supplemental effect of the sodium hydrosulfite on ZnPP formation in the new experimental model was evaluated. The sodium hydrosulfite to was added to a 15 mL sterilized conical tube containing 10 mL of the LTL homogenate (50% (w/w) LTL muscle, pH 5.5, antibiotics added) at a final concentration range of 0-40 mM. After 10 or 20 days of the anaerobic incubation under the darkness described above, the fluorescence intensity of ZnPP/PPIX in each treatment was measured as described in Section 3.2.11.

3.2.8. Evaluation of the heme dissociation amount using HPLC

On each sampling day during anaerobic incubation, each Hb derivative solution was first centrifuged at 20,000 × g for 15 min at 4°C. After removing the supernatant, 1.5 mL of pure water was added into each tube and well mixed. Then, the mixture was centrifuged again at 20,000 × g for 15 min at 4°C and the supernatant was removed. Subsequently, the precipitate of each mixture was mixed with 750 μL of acetic acid/ethyl acetate (1:4 v/v), then allowed to rest on ice for 15 min under the darkness to extract the porphyrins (Wakamatsu *et al.*, 2009). After syringe-filtered through a 0.45 μm cellulose filter (Minisart RC4, Sartorius Stedim Lab Ltd, Stonehouse, UK), the clear supernatant of each mixture was mixed with an equal volume of a mobile phase consisting of 1 M ammonium acetate (pH 5.16)/methanol (16:84, v/v). Immediately after mixing, each sample was applied to an STR ODS-II column (4.6φ × 150 mm, particle size 5 μm; Shinwa Chemical Industries, Kyoto, Japan) with a flow rate of 1.0 ml/min at 35°C, and heme was detected by the absorbance at 400 nm. Besides, since no heme was detected in each second removed supernatant, almost all the dissociated heme from the each Hb derivative was in the precipitate and was measured using this method.

3.2.9. Evaluation of ZnPP formation from hemin-1MI *in vitro*

For evaluating the ZnPP formation from the hemin-1MI *in vitro*, the hemin-1MI solution was first reduced with 20 mM (final concentration) of the ascorbic acid and then added into the incubation buffer (50 μM $ZnCl_2$, 20 mM phosphate buffer at pH 5.5) at a final concentration range of 0-400 μM in a final volume of 1 mL in a 2 mL sterilized microtube. Subsequently, 1 mL of the crude FECH extract, after adjusting pH to 5.5 with

HCl, was quickly added into the microtube. The mixture was ventilated with nitrogen gas for 2 min to purge the oxygen. Next, the microtube of each treatment was transferred into an oxygen-impermeable storage bag with an oxygen absorbent, and incubated at 35℃ under the darkness for 24 h. After incubation, the fluorescence intensity of ZnPP was measured as described in Section 3.2.11. To evaluate the effect of hematin reduction on ZnPP formation no ascorbic acid was added in the solution was set as the control group.

3.2.10. Interaction of hemin-1MI with sodium nitrite, CO, and sodium azide

The evaluate the interaction of hemin-1MI with sodium nitrite, CO, and sodium azide, the hemin-1MI solution was first reduced with 20 mM (final concentration) of ascorbic acid and then added into 20 mM phosphate buffer (pH 5.5) at a final concentration of 125 μM in a final volume of 2 mL in a sterilized microtube. Subsequently, the sodium nitrite was added to the mixture to a 10 mM final concentration for the nitrite treatment, the 10 mL of CO gas was slowly injected to the mixture as the CO treatment. For the azide treatment, the sodium azide was added to the hemin-1MI solution to a 40 mM final concentration, but without a previous reduction by ascorbic acid. Next, all mixtures were ventilated with nitrogen gas for 2 min to purge the oxygen and placed under the darkness for 30 min at room temperature. After reaction, the UV-vis spectrum of each treatment was measured as described in Section 3.2.12.

3.2.11. Fluorescence measurement

The extraction of ZnPP or PPIX in the experimental model and the fluorescence measurement of ZnPP were carried out as described in Chapter 2 Section 2.2.7. The fluorescent intensity of PPIX was measured at 630 nm for excitation at 400 nm. The background fluorescence intensity was eliminated by subtracting the average fluorescence intensity at 610 nm and 650 nm for PPIX measurement to ensure its accurate fluorescence intensities.

3.2.12. UV spectroscopy analysis

The UV absorption spectrum of the new experimental model treated with CO gas or added with sodium azide as well as the hemin-1MI solutions with different treatments were measured as described in Chapter 2 Section 2.2.8.

The UV absorbance of nitrosyl heme in the experimental model, which was added with the sodium nitrite, was measured. After incubation, about 2.5 mL of the new experimental model homogenate was mixed with 7.5 mL of cold acetone and fully mixed then allowed to rest on ice for 30 min under the darkness to extract the nitrosyl heme. After filtering the extract through a filter paper, the nitrosyl heme absorbance at 395 nm (A395) was measured using a UV-vis spectrophotometer equipped with a 1.0 cm quartz cuvette.

3.2.13. Determination of non-heme iron content

The method for the determination of non-heme iron content was same as described in Chapter 2 Section 2.2.12.

3.2.14. SDS-PAGE and western blotting

For the SDS-PAGE, the hand-cast gel was prepared of a 4.5% stacking gel and a 15% separating gel, both of which contained 0.1% sodium dodecyl sulfate (SDS). The apo-Hb solution was mixed 1:1 with a sample buffer (50 mM Tris-HCl (pH 6.8), 4% SDS, 2% 2-mercaptoethanol, 40% glycerol, and 0.3% CBB R-250). Subsequently, the crude FECH extract was denatured by heating for 5 min at 100°C prior to analysis. Electrophoresis was done at 10 mA for 30 min followed by 20 mA for 90 min.

For the gel staining, after electrophoresis, the gel was transferred into a plastic box. After washing the gel three times with pure water, about 50 mL CBB staining solution (0.025% CBB R-250, 30% (v/v) methanol, 10% (v/v) acetic acid) was added, then shook for one hour at room temperature. The gel was next washed three times with pure water, and the pure water was used for destaining overnight at room temperature.

For the western blotting analysis of FECH, the detail operation steps of were described in Chapter 2 Section 2.2.10. After transfer, the PVDF membrane was reacted with rabbit polyclonal anti-FECH (2,000-fold dilution, Abcepta, Inc., San Diego, California, USA) for 14 h at 4°C. Next, horseradish peroxidase (HRP)-conjugated anti-rabbit IgG (10,000-fold dilution, Jackson Immuno Research Laboratories, West Grove, Pennsylvania, USA) was reacted with the membrane for 2 h at 4°C.

3.2.15. Statistical analysis

The statistical analysis was carried out with JMP Pro software version 16.1.0 (SAS Institute Inc., Cary, North Carolina, USA). Data were expressed as the mean ± SEM of three independent repetitions. The unpaired Student's t-test was used to perform two-group comparisons. A one-way ANOVA with Tukey's multiple comparison test was performed to evaluate the difference among groups. Statistical significance was set at $p < 0.05$.

3.3. Results

3.3.1. Supplemental effects of sodium nitrite, sodium azide, and CO on the ZnPP formation in the experimental model

To verify that whether NO, azide, and CO as ligands binding to endogenous heme proteins and whether their existences in meat homogenate affect the formation of ZnPP, the sodium nitrite, sodium azide, and CO was separately added to the new experimental model.

After incubation, The CO-heme specific absorbance spectrum was observed in the new experimental model with CO added (Fig. 13). With the increasing of sodium azide added to the new experimental model, the Soret peak and Q bands of endogenous heme proteins were red-shifted to those of azide-heme, and increased (Fig. 14 arrows). Meanwhile, the amount of the formed nitrosyl heme increased with the addition of sodium nitrite to the new experimental model, and reached in the maximum level at sodium nitrite over 40 μM (Fig. 15A). Therefore, the NO, azide, and CO could bind with the endogenous heme proteins to form various heme protein derivatives in meat homogenate.

On the other hand, the addition of sodium nitrite suppressed the formation of ZnPP in the new experimental model in a dose-dependent manner, and with the addition of sodium nitrite over 40 μM, ZnPP formation reduced in a plateau (Fig. 15A). The formation of ZnPP in the CO-treated group was significantly lower ($p < 0.01$) than that in the control group (Fig. 15B). Moreover, with the addition of sodium azide, ZnPP formation was gradually suppressed in the new experimental model, reaching a minimum level at 4 mM sodium azide added (Fig. 15C). Therefore, the conversion of the endogenous heme proteins to their derivatives induced by NO, azide, and CO could inhibit ZnPP formation in meat homogenate. However, it is possible that they affected meat components other than endogenous heme proteins to inhibit ZnPP formation.

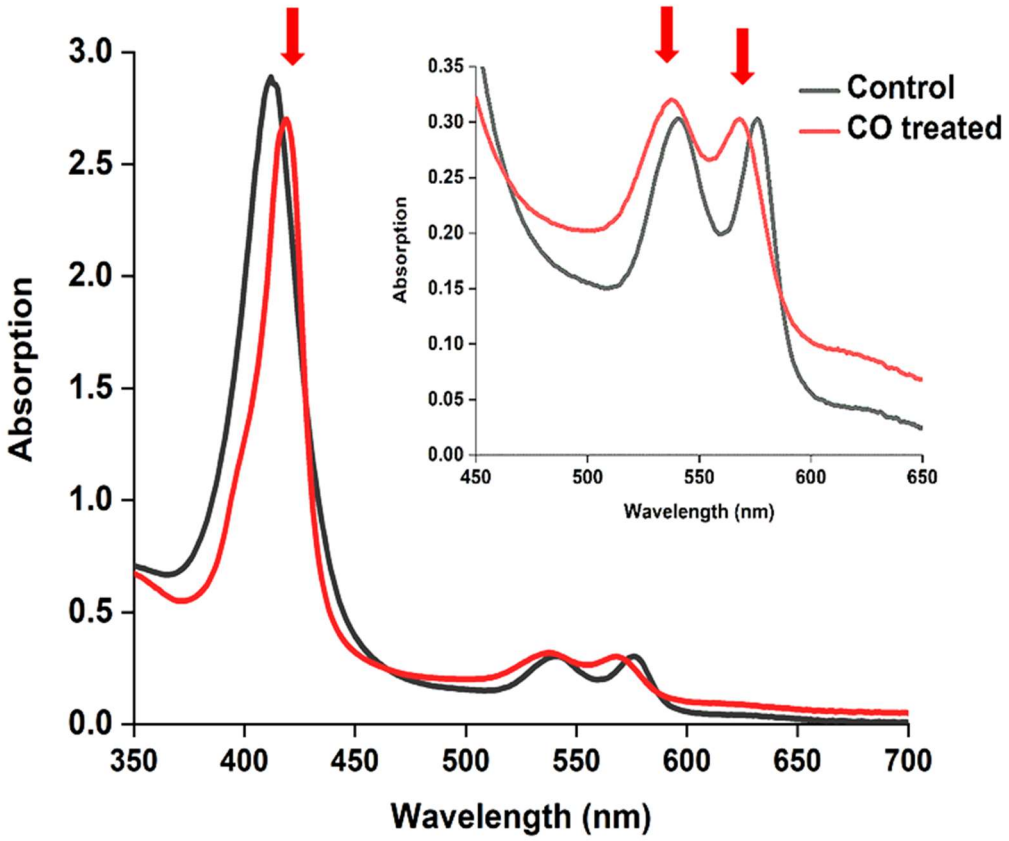

Fig. 13. UV-visible absorption spectrum of the new experimental model supernatant treated with CO gas

The UV-visible absorption spectrum of the new experimental model supernatant, treated with CO gas, were observed after anaerobic incubation. Control: the new experimental model supernatant without the CO treatment. The inserted image shows the enlarged spectra of the specific Q bands. The arrows indicate peaks, which were shifted by the treatment with CO.

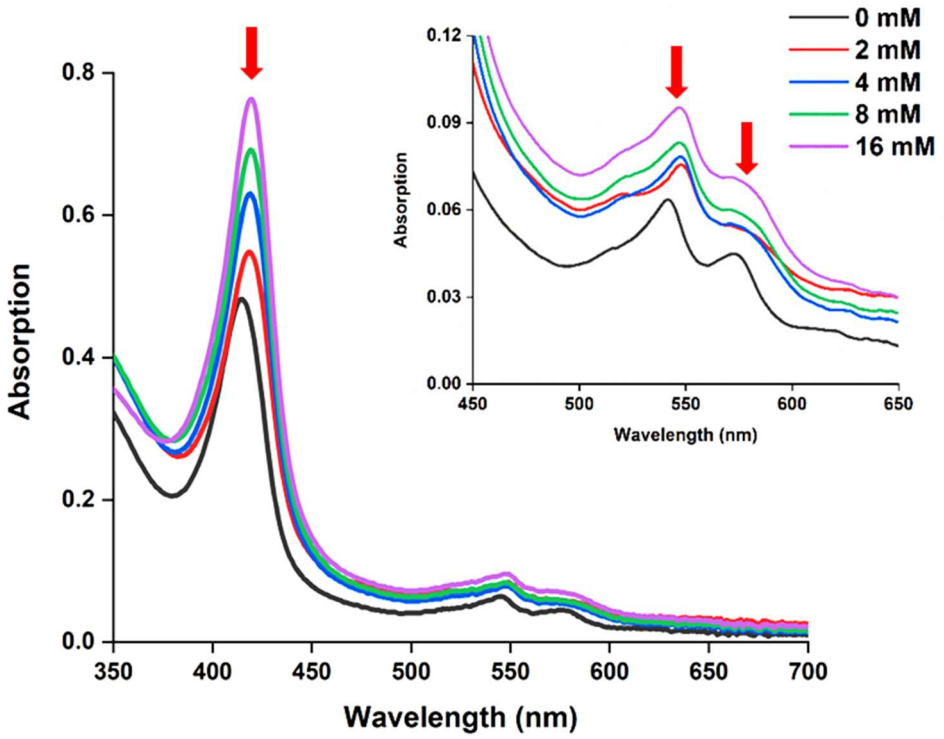

Fig. 14. UV-visible absorption spectrum of the new experimental model supernatant with different concentration of sodium azide addition

The UV-visible absorption spectrum of the new experimental model supernatant with the addition of sodium azide of 0-16 mM final concentration was observed after anaerobic incubation. The inserted image shows the enlarged spectra of the specific Q bands. The arrows indicate peaks, which were shifted by the addition of sodium azide.

Fig. 15. Effects of sodium nitrite (A), CO (B), and sodium azide (C) on the formation of ZnPP in the new experimental model after incubation

The sodium nitrite, CO gas, and the sodium azide were added to the new experimental model, the ZnPP fluorescence intensity of each group was measured. After 10 days anaerobic incubation at 35℃, in the sodium nitrite added group, the absorbance of the nitrosyl heme Soret peak was also observed (A, ▼). Values are means ± SEM (n = 3); ^{abcd}: Values with different letters indicate the significant differences in ZnPP formation ($p < 0.05$); ^{xyz}: Values with different letters indicate the nitrosyl heme absorbance is significantly different ($p < 0.05$); **: $p < 0.01$.

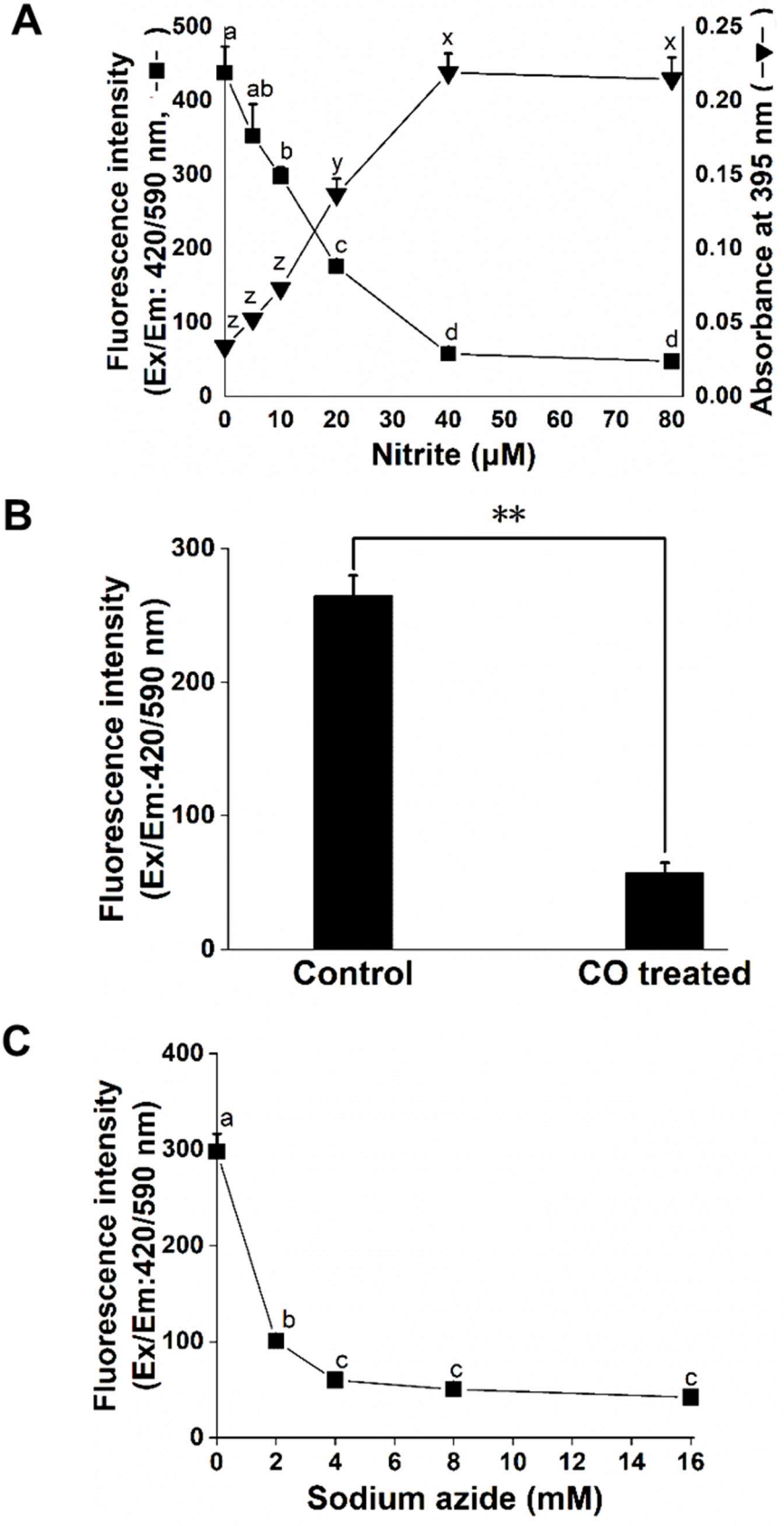
A
Fluorescence intensity (Ex/Em: 420/590 nm, -■-)
Absorbance at 395 nm (-▼-)
Nitrite (μM)
a
ab
b
c
d
x
y
z
B
**
Fluorescence intensity (Ex/Em:420/590 nm)
Control
CO treated
C
Fluorescence intensity (Ex/Em:420/590 nm)
Sodium azide (mM)

3.3.2. Supplemental effects of various Hb derivatives on ZnPP formation in the experimental model

To eliminate the effect of each ligand molecule to the endogenous components except to heme proteins, such as FECH, on ZnPP formation in meat homogenate under anaerobic conditions, the prepared OxyHb, NOHb, COHb, and N_3mHb derivatives were separately added into the new experimental model as the exogenous heme substrate with an equal final concertation. The changes in ZnPP, PPIX, and released non-heme iron content in each group were monitored during anaerobic incubation (Fig. 16). The accumulation of ZnPP, PPIX, and released non-heme iron during anaerobic incubation in all groups was observed, which was produced from the endogenous heme proteins in meat homogenate (Fig. 16). However, only the addition of OxyHb showed a significant higher ZnPP formation during anaerobic incubation compared with that in control group in which no exogenous Hb was added (Fig. 16A). The addition of NOHb, COHb, or N_3mHb did not show a significant higher ZnPP formation compared with the control group. Moreover, in the OxyHb-added group, during anaerobic incubation, the formation of PPIX and released non-heme iron also increased significantly ($p < 0.05$) compared with other groups, whereas no significant difference in their formation was observed among NOHb-added, COHb-added, N_3mHb-added, and control groups (Fig. 16 B and C). The increasing trends of both PPIX and released non-heme iron formation in each group were consistent with those in the ZnPP increases during anaerobic incubation (Fig. 16). These results suggested that the addition of various Hb did not affect the ZnPP formation from the endogenous heme proteins, whereas the heme in NOHb, COHb, and N_3mHb could not be deironized for ZnPP/PPIX formation under anaerobic conditions.

3.3.3. Heme dissociation amount from various exogenous Hb derivatives during anaerobic incubation

The changes in the heme dissociation amount from OxyHb, NOHb, COHb, and N_3mHb derivatives were monitored during anaerobic incubation (Table 3). On day 0, almost no dissociated heme was detected among all the Hb derivatives. For the OxyHb derivative, the heme dissociation amount was constantly increasing throughout the period of the

Fig. 16. Supplemental effects of exogenous OxyHb, NOHb, COHb, and N_3mHb on ZnPP formation (A), PPIX formation (B), and released non-heme iron (C) in the new experimental model during anaerobic incubation

After the addition of the exogenous various Hb derivatives in the new experimental model, the ZnPP formation, PPIX formation, and the released non-heme iron of each group were monitored during anaerobic incubation. OxyHb: 0.005% (w/w) OxyHb-added group; NOHb: 0.005% (w/w) NOHb-added group; COHb: 0.005% (w/w) COHb-added group. N_3mHb: 0.005% (w/w) N_3mHb-added group. Values are means ± SEM (n = 3). ^{abcde}: values with different letters within the same group indicate the significant differences during anaerobic incubation; ^{xy}: values with different letters within the same incubation day indicate the significant differences among groups ($P < 0.05$).

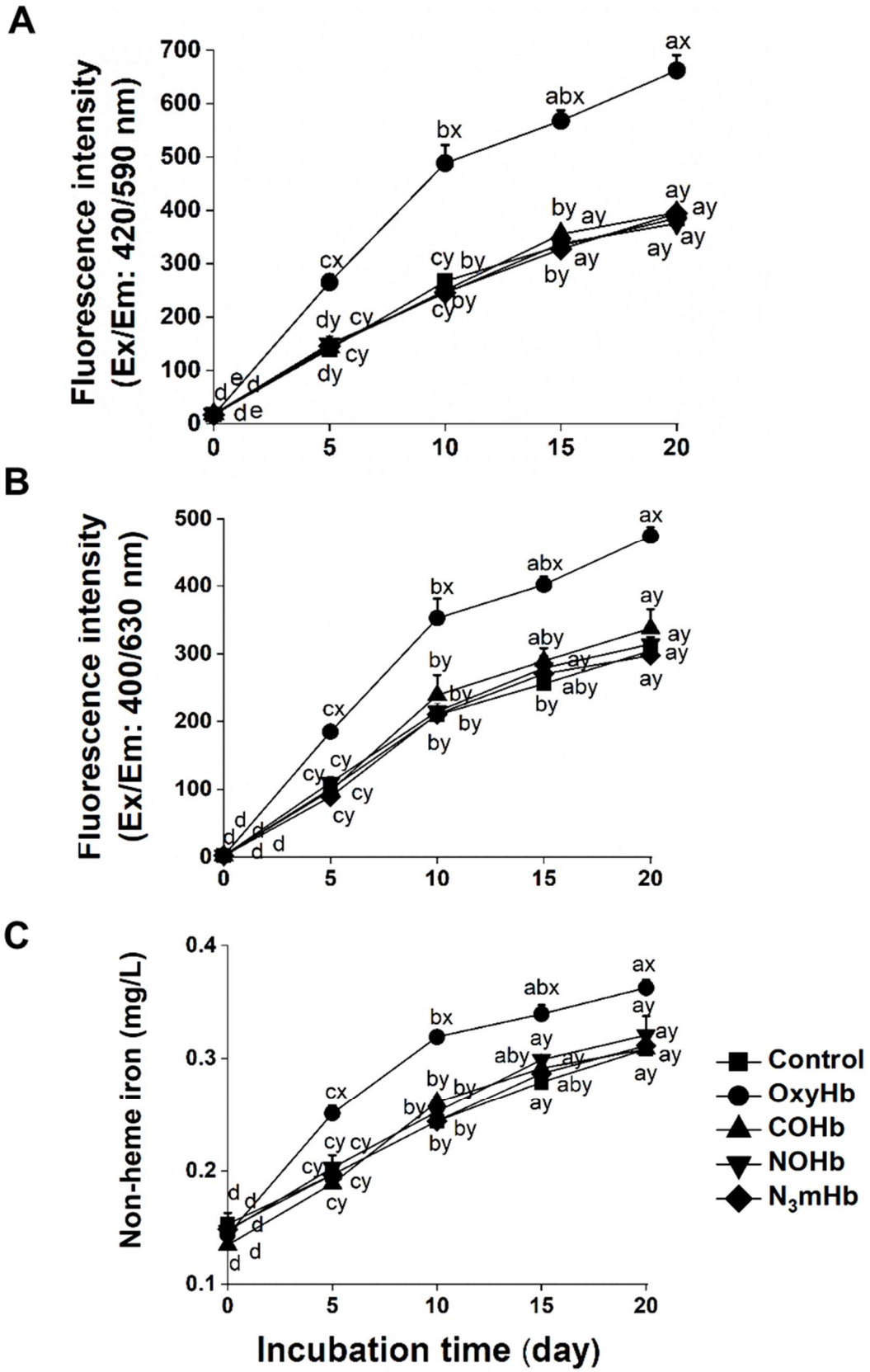
A
Fluorescence intensity (Ex/Em: 420/590 nm)
B
Fluorescence intensity (Ex/Em: 400/630 nm)
C
Non-heme iron (mg/L)
Incubation time (day)
Control
OxyHb
COHb
NOHb
N3mHb

anaerobic incubation, and reached a maximum concentration at 4.878 μg/mL after 20 days anaerobic incubation. In contrast, the heme dissociated contents of NOHb, COHb, and N_3mHb derivatives increased slightly compared with the OxyHb derivative, and were much lower than that of OxyHb derivative during anaerobic incubation. In addition, the heme dissociated content among NOHb, COHb, and N_3mHb derivatives showed no significant difference over the anaerobic incubation. Therefore, it was suggested that the heme was hard to dissociate from the NOHb, COHb, and N_3mHb derivatives under the anaerobic conditions compared with the OxyHb derivative.

Table 3. The heme contents dissociated from OxyHb, COHb, NOHb, and N_3mHb derivatives during anaerobic incubation (μg/mL).

	OxyHb	NOHb	COHb	N_3mHb
Day 0	0.0028 ± 0.0001^{e}	0.0030 ± 0.0001^{c}	0.0037 ± 0.0014^{d}	0.0023 ± 0.0001^{c}
Day 5	0.9379 ± 0.0506^{dx}	0.1144 ± 0.0029^{byz}	0.2305 ± 0.0151^{cy}	0.0040 ± 0.0001^{cz}
Day 10	2.1322 ± 0.0151^{cx}	0.1388 ± 0.0053^{aby}	0.2779 ± 0.0107^{bcz}	0.0168 ± 0.0017^{by}
Day 15	3.8108 ± 0.0984^{bx}	0.1447 ± 0.0074^{ay}	0.3569 ± 0.0078^{ayz}	0.0406 ± 0.0027^{az}
Day 20	4.8778 ± 0.2006^{a}	0.1475 ± 0.0075^{ay}	0.3584 ± 0.0038^{ayz}	$0.0426 \pm 0 .0020^{az}$

Values are means ± SEM (n = 3). ^{abcde}: values with different letters within the same group indicate the significant differences during anaerobic incubation ($p < 0.05$); ^{xyz}: values with different letters within the same incubation day indicate the significant differences among groups ($p < 0.05$).

3.3.4. Protein structural stability of various Hb derivatives during anaerobic incubation

In order to evaluate the protein structural stability of OxyHb, NOHb, COHb, and N_3mHb during anaerobic incubation, the changes in absorbance spectra and Trp fluorescence spectra in various Hb derivatives were observed (Fig. 17 and 18).

The absorbance spectra of OxyHb showed a blue shift in the Soret band peak from the 415 nm to the 405 nm region after 5 days of anaerobic incubation, and the Soret band peak of OxyHb continue to decrease over the incubation time (Fig. 17A). The Soret band peak in the 405 nm region has been attributed to the absorbance of mHb, and the typical Q bands of OxyHb (541 nm and 577 nm) were decreased and shifted to 500 nm and 631 nm during anaerobic incubation, which also consistent with those of mHb. On the other hand, little change was detected in the Soret band peak and Q bands of NOHb (Fig. 17B), COHb (Fig. 17C), and N_3mHb (Fig. 17D) derivatives, indicating their heme-globin bindings were stable during anaerobic incubation.

Furthermore, the Trp fluorescence intensity of OxyHb was increased during anaerobic incubation (Fig. 18A), especially a notable increase was observed in the first 10 days of anaerobic incubation. As for other Hb derivatives, little increase in the Trp fluorescence intensities was recorded in NOHb (Fig. 18B), COHb (Fig. 18C) and N_3mHb (Fig. 18D) derivatives. Therefore, compared with the OxyHb derivative, the NOHb, COHb, and N_3mHb derivatives showed little globin protein unfolding under the anaerobic conditions.

3.3.5. Effects of the free heme and its reduction on ZnPP formation *in vitro*

To confirm whether the heme dissociated from heme proteins could be used as the precursor to form ZnPP by the interaction with FECH, the hemin-1MI solution, which was prepared by dissolving the hemin standard into the aqueous buffer, was incubated anaerobically with the crude FECH extract and zinc ions. After the addition of ascorbic acid in hemin-1MI solution for the heme reduction reaction, ZnPP formation dose-dependently increased between 0 and 200 μM of the added reduced hemin-1MI solution, and the further increase was not significant (Fig. 19). Next, to confirm whether the heme reduction is essential for ZnPP formation, the hemin-1MI solution was separately incubated anaerobically with the incubation mixture under two conditions, with or

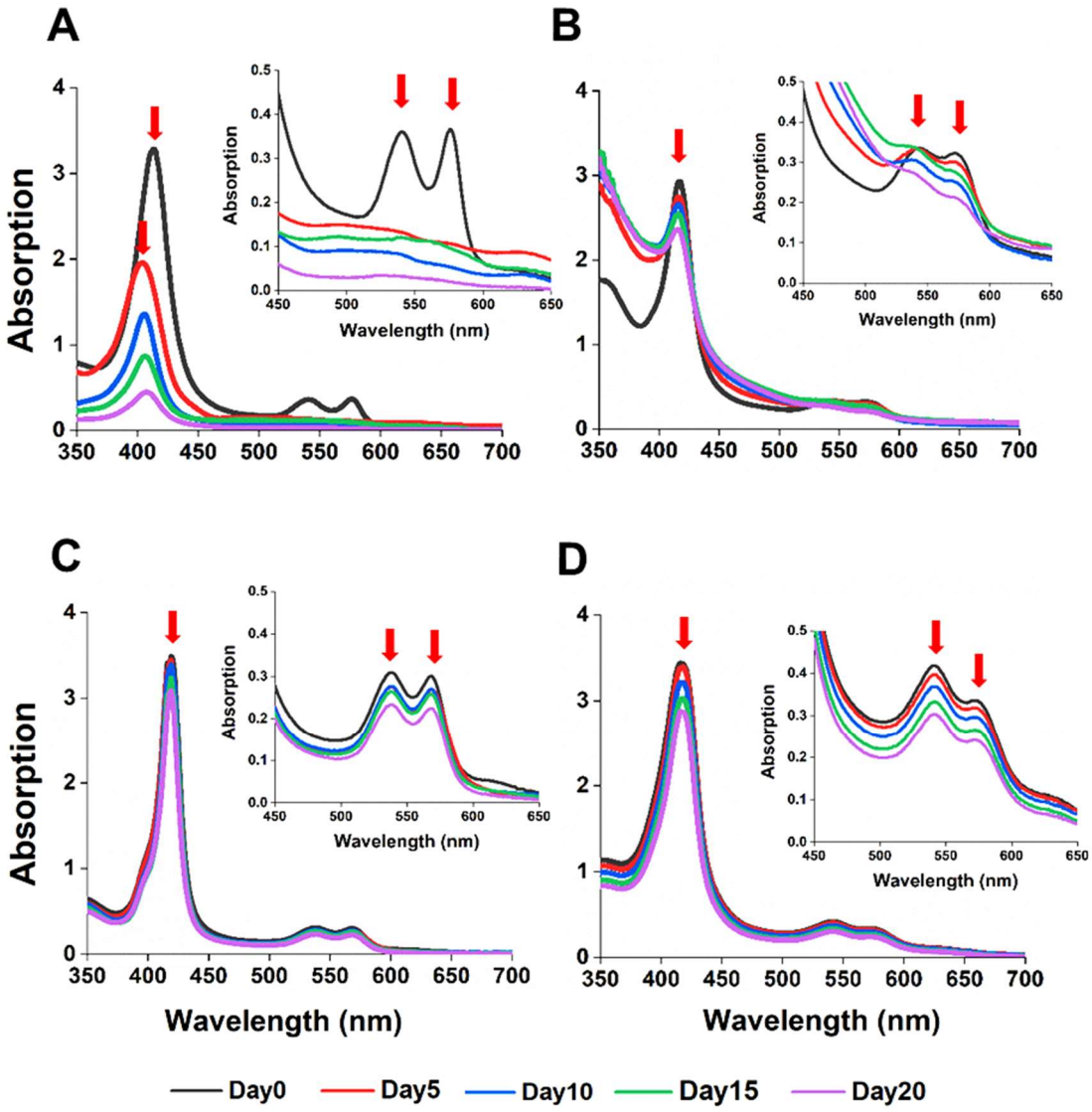

Fig. 17. Changes in the UV–vis spectra of OxyHb (A), NOHb (B), COHb (C), and N_3mHb (D) derivatives during anaerobic incubation

The UV–vis spectra spectrum of each Hb derivative was observed during anaerobic incubation. The inserted image shows the enlarged spectra of the specific Q bands. The arrows indicate peaks, which were changed during anaerobic incubation.

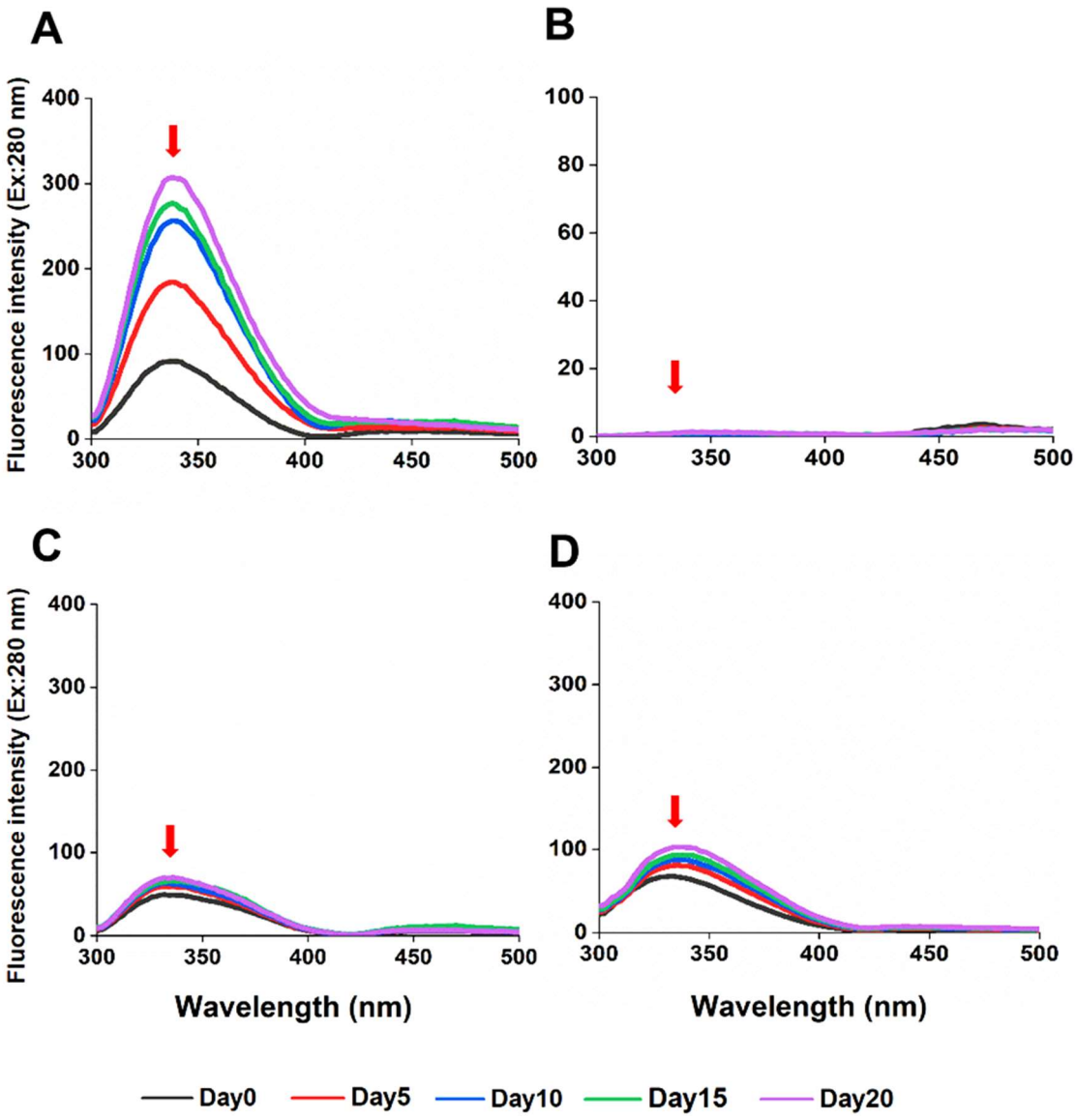

Fig. 18. Changes in the fluorescence spectrum derived from the Trp in OxyHb (A), NOHb (B), COHb (C), and N_3mHb (D) during anaerobic incubation

The fluorescence spectrum derived from the Trp of each Hb derivative was observed at the excitation wavelength of 280 nm during anaerobic incubation. The arrows indicate the Trp-derived fluorescence, which was changed during anaerobic incubation.

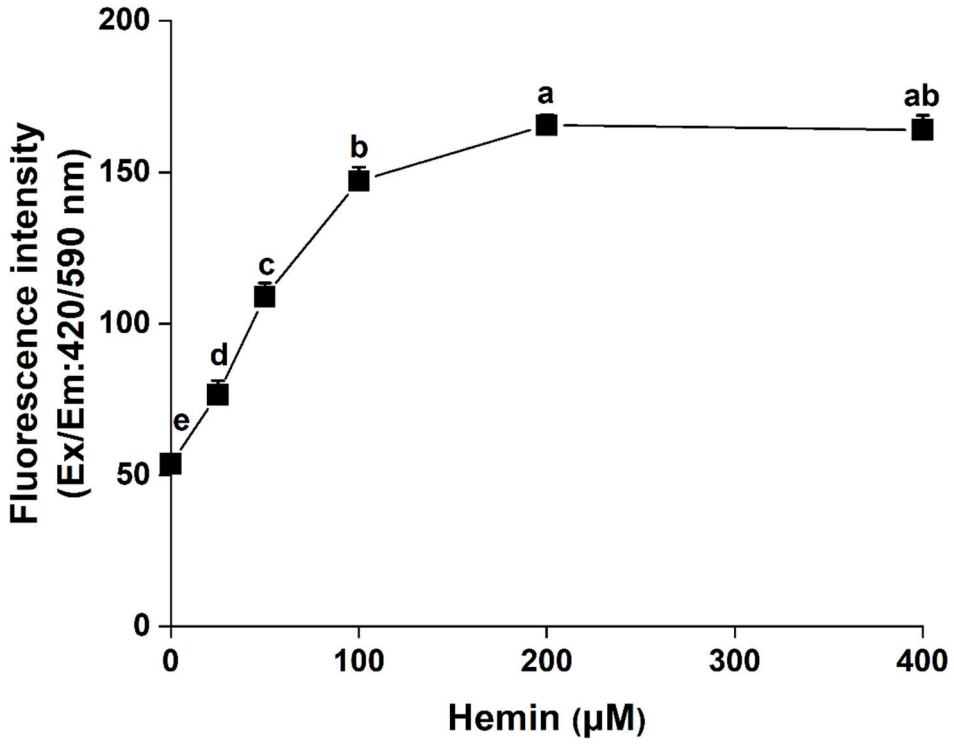

Fig. 19. Effect of the ZnPP formation from hemin-1MI

The effect of hemin-1MI solution addition in the incubation mixture on ZnPP formation was evaluated after anaerobic incubation. Values are means ± SEM (n = 3). ^{abcde}: ZnPP formation is significantly different in different hemin-added groups ($p < 0.05$).

without the addition of ascorbic acid as the reductant before incubation (Fig. 20). As a result, ZnPP was not formed without the reduction of hematin to heme induced by ascorbic acid, whereas ZnPP increased significantly when ascorbic acid was added to reduce hematin to heme. Therefore, the reduction of the free hematin to heme was essential for ZnPP formation.

3.3.6. Effect of the over reduction on ZnPP formation

To confirm whether the over reduction inhibited ZnPP formation in meat, the sodium hydrosulfite was added to the new experimental model as a strong reductant. After anaerobic incubation, with the addition of sodium hydrosulfite increased from the final concentration range of 0-10 mM, the formation of ZnPP was increased (Fig. 21). However, a notable decrease in ZnPP was recorded when more (20- and 40-mM final concentrations) sodium hydrosulfite was added (Fig. 21). Therefore, the excessive reductant inhibited ZnPP formation in meat.

3.3.7. Effects of the sodium nitrite addition, CO treatment, and sodium azide addition on the free heme/hemin

To confirm whether the addition of sodium nitrite or sodium azide, and the treatment of CO could derive ligands binding to the free heme/hematin, the UV-vis spectrum of the heme/hemin-1MI solution after different treatments were observed. Compared with control group, which was only the hemin-1MI solution without any treatment, no heme absorption spectrum changes were observed among all treated groups (Fig. 22). Therefore, the NO, azide, and CO ligands could not bind to the free heme/hematin.

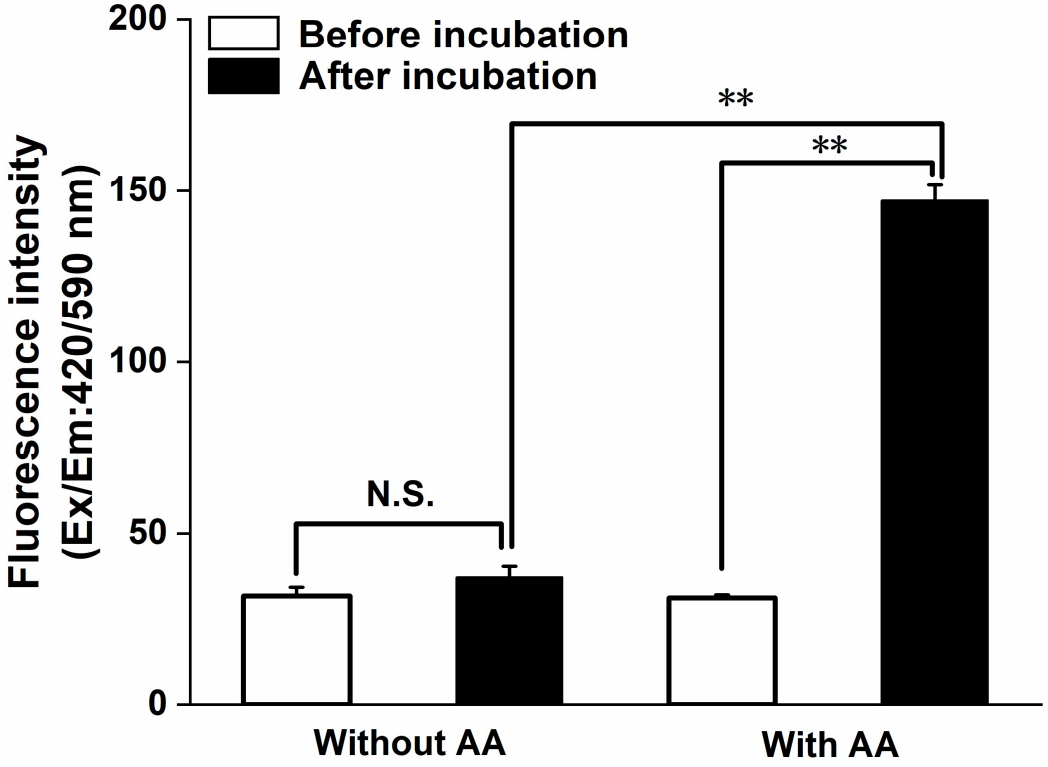

Fig. 20. Effect of ascorbic acid addition on ZnPP formation from hemin-1MI

Ascorbic acid solution was added into the hemin-1MI solution as the reductant, before and after anaerobic incubation, the ZnPP fluorescence intensity in both with and without the ascorbic acid-added groups were measured. With AA: ascorbic acid was added to 100 μM hemin-1MI solution with 20 mM final concentration. Values are means ± SEM (n = 3). N.S.: $p > 0.05$; **: $p < 0.01$.

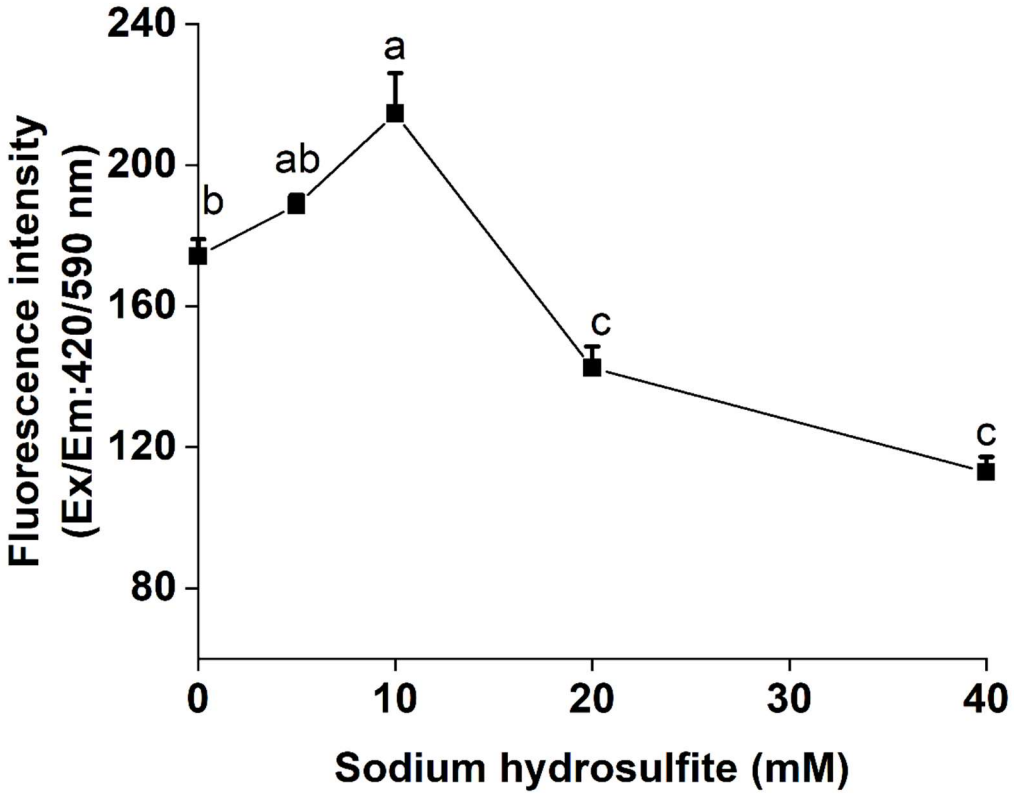

Fig. 21. Effect of the sodium hydrosulfite on ZnPP formation

Sodium hydrosulfite was added dose-dependently into the new experimental model as the reductant, after anaerobic incubation, the ZnPP fluorescence intensity was measured. Values are means ± SEM (n = 3). ^{abc}: ZnPP formation is significantly different in different sodium hydrosulfite-added groups ($p < 0.05$).

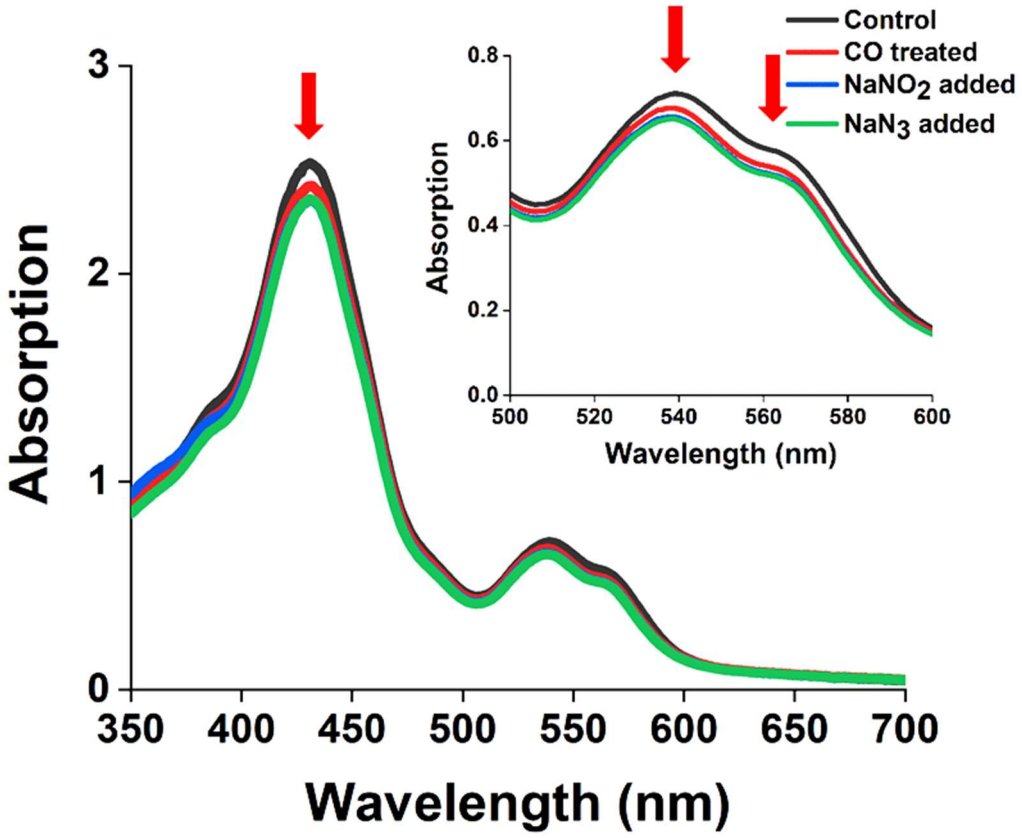

Fig. 22. UV-vis spectrum of the heme-1MI solutions after different treatments

Sodium nitrite, CO, and sodium azide were added to the heme-1MI solution (0.125 mM), after reaction, the UV-vis spectra of each treatment observed in the range of 350–700 nm. Control: heme-1MI solution without any treatment; CO treated: heme-1MI solution treated the CO gas; $NaNO_2$ added: sodium nitrite was added to the heme-1MI solution to a 10 mM final concentration; NaN_3 added: sodium azide was added to the hemin-1MI solution to a 40 mM final concentration. The inserted image shows the enlarged spectra of the specific Q bands of hemin-1MI. The arrows indicate the characteristic peaks of hemin-1MI.

3.4. Discussion

In this chapter, to elucidate the significance of heme dissociation from heme proteins on ZnPP formation, the inhibitory mechanism of nitrite on ZnPP formation in meat was investigated by using CO and sodium azide as comparisons. The significance of reduction reaction of the dissociated heme and the over reduction effect on ZnPP formation was also evaluated.

The results obtained from this chapter revealed that the addition of CO to the meat homogenate significantly suppressed ZnPP formation under anaerobic conditions (Fig. 15B). From the results in Chapter 2, due to the unstable heme-globin binding of Hb, the heme, dissociated from Hb, was suggested as the main precursor for ZnPP formation in meat. Meanwhile, the mammalian FECH, which has a [2Fe–2S] cluster around its active site, was reported to be involved in the conversion of dissociated heme to ZnPP (Chau *et al.*, 2010, 2011; Sellers *et al.*, 1996). Since the treatment of CO could not causes disassembly of the FECH [2Fe-2S] cluster (Sellers *et al.*, 1996) unlike NO, the inhibition of CO on ZnPP formation in meat was suggested to suppress the heme dissociation from Hb. It has been reported that CO has a strong affinity for the heme (Fe^{2+}) of Hb to convert it to COHb (Deatherage *et al.*, 1979), and the absorption spectrum of CO-heme was also observed in the meat homogenate after CO treatment (Fig. 13). The stereochemistry of the CO-heme complex in COHb is significantly strained (Deatherage *et al.*, 1979), which might result in a stable heme-globin binding of COHb (Fig. 17C and 18C). Thus, heme was hard to dissociate from the heme pocket of COHb, and the heme iron in COHb was hard to be removed to convert heme to PPIX as the ZnPP-forming precursor (Table 3, Fig. 16) because it was linked in the stable CO-heme complex in COHb. In addition, CO as the heme ligand did not bind to the free heme, which was reduced from the hemin-1MI by ascorbic acid (Fig. 22), indicating that CO inhibited ZnPP formation by binding to the heme in Hb rather than binding to the free heme dissociated from Hb. Therefore, CO inhibited ZnPP formation in meat by binding to the heme (Fe^{2+}) of endogenous Hb to suppress its heme dissociation and heme iron-removal reaction, demonstrating that the heme (Fe^{2+}) dissociated from the endogenous Hb and then converted to ZnPP *via* PPIX was significant for ZnPP formation in meat.

On the other hand, the addition of sodium azide to the meat homogenate was observed to dose-dependently inhibit ZnPP formation under anaerobic conditions (Fig. 15C). It has been reported that the heme dissociation rate of heme proteins is related to their oxidation (Hargrove *et al.*, 1994). Since reducing enzymes for Hb are located in erythrocytes, the Hb outside of erythrocytes is easily autoxidized to mHb and then dissociated hematin (Hargrove *et al.*, 1994). However, the azide anion can bind to the hematin (Fe^{3+}) of the mHb (Fig. 14) at an angle Fe-N-N of 125° to form the N_3mHb, which showed a low interference in the protein structure and slightly contracted the ligand pocket (Deatherage *et al.*, 1979). This binding conformation provide a stable hematin-globin binding of N_3mHb during anaerobic incubation (Fig. 17D and 18D), and made hematin be wrapped in the heme pocket of N_3mHb, resulting in less hematin dissociated from the heme pocket of N_3mHb (Table 3). In addition, the stable azide-hematin binding structure suppressed the heme iron of N_3mHb be removed to convert hematin to PPIX as the ZnPP-forming precursor in meat (Fig. 16). Same as CO ligand, the azide did not bind to the dissociated hematin to form the free azide-hematin complex (Fig. 22). Therefore, sodium azide inhibited ZnPP formation in meat because the azide anion bound to the hematin (Fe^{3+}) of endogenous autoxidized mHb to suppress its hematin dissociation and heme iron-removal reaction, demonstrating that the hematin (Fe^{3+}) dissociated from the endogenous autoxidized heme proteins and then converted to ZnPP *via* PPIX was also important for ZnPP formation in meat.

Similarly, NO derived from the sodium nitrite added to the meat homogenate inhibited ZnPP formation under anaerobic conditions (Fig. 15A). Since the NO could destroy the [2Fe–2S] cluster of the mammalian FECH (Furukawa *et al.*, 1995), the NO derived from nitrite might inhibit ZnPP formation by suppressing the FECH catalytic activity of iron removal and the zinc insertion. On the other hand, as mentioned above, the heme dissociated from heme proteins, especially Hb, was significant for ZnPP formation in meat. Thus, NO reacted with heme proteins to form the stable nitrosyl heme proteins (Fig. 15A), especially the NOHb, might inhibit ZnPP formation in meat by suppressing its heme dissociation. Similar to CO, NO as a kind of monoxide heme ligands could rapidly associates with either the α or β subunit of the R-state Hb to form the NOHb (Yi *et al.*, 2008). In the α subunit, the NO binds to the iron of heme (Fe^{2+}), and the hydrogen bonds

between the nitrite ligand and the distal His residues of Hb are reported as two modes, like Fe-N-His87 and Fe-O-His58. In addition, in the β subunit, there are also two NO binding modes, which are Fe-N-His92 and Fe-O-His63 (Yi *et al.*, 2008). Moreover, after Hb autoxidized to the mHb in meat, not only azide anion could bind to the mHb, NO can also bind to the iron of hematin (Fe^{3+}) in mHb to form the NOHb, which showed almost no pronounced distortion of the NO-hematin and maintained structural stability (Deatherage *et al.*, 1979). These binding conformations made heme/hematin stabilize in the heme-globin binding of NOHb (Fig. 17B and 18B), and the heme/hematin were hard to dissociated from its heme pocket during anaerobic incubation (Table 3). Also, similar to COHb and N_3mHb, the heme iron was maintained in the NO-heme/hematin complex of NOHb and was rarely removed from NOHb to convert heme/hematin to ZnPP *via* PPIX (Fig. 16). In addition, NO did not bind with the free heme to form the NO-heme complex, which was consistent with CO and azide ligands (Fig. 22). Therefore, in addition to inhibiting ZnPP formation by suppressing the FECH catalytic activity of iron removal and the zinc insertion, NO could also inhibit ZnPP formation in meat by binding to endogenous Hb/mHb to suppress their heme/hematin dissociation and heme iron-removal reaction, which indicated that the heme/hematin dissociated from endogenous heme proteins and then converted to ZnPP *via* PPIX was significant for ZnPP formation in meat.

Furthermore, the reduction of the free hematin was found to be essential for ZnPP formation (Fig. 19 and 20), whereas the excessive reductant addition significantly suppressed the formation of ZnPP in meat homogenate (Fig. 21). It has been reported that Hb leaked from the erythrocytes after hemolysis was highly cytotoxic due to its ability to catalyze free radical formation (Ascenzi *et al.*, 2005). Thus, a heme scavenging system was existed for the Hb clearance (Ascenzi *et al.*, 2005), and the release of hematin (Fe^{3+}) was proposed as a part of the heme scavenging system of Hb (Wakamatsu, 2022). On the other hand, the Hb in meat was easily autoxidized to the mHb due to the lack of Hb reducing enzyme, resulting in a large amount of hematin dissociated form the unstable heme-globin binding of mHb (Table 3, Fig. 17A and 18A). In contrast, less hematin was proposed to dissociate from the oxidized metMb because it has multiple reduction pathways in meat (Ramanathan *et al.*, 2020). Thus, a large amount of hematin could dissociate from mHb, and the dissociated hematin was observed to contribute to ZnPP

formation in meat homogenate (Fig. 16A). However, the mammalian FECH showed only the ability to catalyze the removal of iron from heme to form PPIX as the ZnPP-forming precursor, and the addition of Fe^{3+} notably suppressed this iron-removal reaction (Chau *et al.*, 2010). Consistently, without reducing hematin to heme by reductants, such as NADH and ascorbic acid, the mammalian FECH was unable to catalyze the conversion of free hematin to ZnPP *in vitro* experiment (Fig. 20) (Taketani *et al.*, 2007). Thus, a reduction of the dissociated hematin in meat by the endogenous reductases, such as myoglobin reductase, was proposed to be previously needed for ZnPP formation. However, the excess reductant addition was observed to suppress the formation of ZnPP in meat homogenate (Fig. 21), which was speculated as the over reduction mainly prevented the autoxidation of Hb to mHb, resulting in less hematin dissociation from mHb. Therefore, after the hematin dissociated from endogenous autoxidized heme proteins, a following reduction of the free hematin to heme catalyzed by the endogenous reductases was proposed to be previously needed for ZnPP formation in meat. In addition, the over reduction is speculated to suppress ZnPP formation by preventing the autoxidation of endogenous Hb in meat.

Additionally, some researches have been reported that there is a little or no ZnPP was formed in meat products cured with nitrite (Adamsen *et al.*, 2006; Laursen *et al.*, 2008; Wakamatsu *et al.*, 2010). According to the previous study (Wakamatsu *et al.*, 2010) and the results in this chapter, the feasible inhibitory mechanism of nitrite on ZnPP formation in the nitrified dry-cured meat products was suggested as follows. When nitrite added to the meat, it was reduced and converted into NO (Shimizu *et al.*, 2015). NO inhibited ZnPP formation in meat by degrading the [2Fe–2S] cluster of the mammalian FECH, resulting in FECH losing the activity to catalyze the iron-removal reaction of free heme to form PPIX and catalyze zinc insertion into PPIX to form ZnPP. In addition, NO as the heme ligand strongly bound to the heme iron in endogenous heme proteins to convert them to the nitrosyl heme proteins. Since the formed NO-heme complex was stabilized in the heme-globin structure of nitrosyl heme proteins, heme was hard to dissociate from their heme pocket and the heme iron was hard to be removed from the NO-heme complex to convert heme to ZnPP *via* PPIX. Therefore, nitrite was proposed to inhibit ZnPP

formation in the nitrified dry-cured meat products by suppressing the dissociation of heme from heme proteins as well as the degradation of a [2Fe-2S] cluster in FECH.

In conclusion, this chapter revealed the heme dissociated from endogenous heme proteins was significant for the formation of ZnPP *via* PPIX in meat. In addition, the reduction of the dissociated hematin to heme by meat-inherent reductases was suggested to be previously needed to form ZnPP, but the over reduction may suppress ZnPP formation by preventing the autoxidation of endogenous heme proteins.

Chapter 4

General discussion

In this study, to elucidate the formation mechanism of ZnPP from heme proteins in the nitrite/nitrate-free dry-cured meat products, the mechanism of Hb as the significant substrate to form ZnPP and the formation pathway of the ZnPP-Hb were investigated using a newly established experimental model. In addition, the significance of the heme dissociation from heme proteins on ZnPP formation was elucidated by investigating the inhibitor pathway of nitrite on ZnPP formation in meat. Also, the potential formation pathway of the ZnPP-Mb in meat was proposed.

4.1. Hb is the significant substrate for ZnPP formation in meat

In the present study, the exogenous addition of Hb in the new experimental model significantly promoted the formation of the ZnPP compared with exogenous Mb addition (Fig. 8A), indicating Hb was the better substrate than Mb to form ZnPP in meat. Since the heme derived from heme proteins was considered as the precursor to form ZnPP, Mb was always proposed as the main substrate to form ZnPP (Khozroughi *et al.*, 2019) because it is the most abundant heme proteins in meat (Ledward, 1992). In contrast, in most meat, Hb only constituted about 10-20% of the total heme proteins (Ledward, 1992). However, the property of readily dissociated heme of Hb might be the reason why Hb was the favorable substrate for ZnPP formation compared with Mb in meat. Different from Mb, which was a sarcoplasmic protein that existed in meat, Hb generally encapsulated in the erythrocytes as a tetrameric form (Pennell, 1964). After slaughter, erythrocytes immediately hemolyze and the hemolysates penetrate the capillary walls to enter the surrounding muscle tissues (Warriss, 1977). The most tetrameric Hb of the hemolysates leaked from the erythrocytes was converted into its dimeric form (Schaer *et al.*, 2014), which caused the release of a large amount of heme from the exposure heme pocket of Hb dimer (Hargrove *et al.*, 1997; Huang *et al.*, 2013). In addition, compared with Mb, the heme-7-propionate in Hb could not link to nearby surface amino acids residues to form a stable heme-globin structure (Cai *et al.*, 2016; Hargrove *et al.*, 1994). Thus, the unstable heme-globin binding of Hb was thought to result in the heme

dissociation from the heme pocket of Hb was much higher than that from Mb (Fig. 8C, 9, and 10). Although proteolysis was suggested as the additional pathway of heme dissociated from heme proteins to form ZnPP (Grossi *et al.*, 2014), some reports proposed it was not essential because ZnPP formation was observed without heme protein degradation (Wakamatsu *et al.*, 2019; Wang *et al.*, 2021). Therefore, the hemolyzed Hb dimer was considered as the favorable substrate for ZnPP formation rather than Mb in meat because heme was more easily dissociated from Hb dimer than from Mb as the precursor to form ZnPP.

Additionally, it has been reported that the heme dissociation rate of heme proteins is related to their oxidation (Hargrove *et al.*, 1994). The metMb oxidized from Mb could be rapidly reduced in meat *via* enzymatic, non-enzymatic, and electron-transport pathways (Ramanathan *et al.*, 2020). However, the Hb outside of erythrocytes, lacking the Hb reducing enzymes, is easily autoxidized to the mHb (Schaer *et al.*, 2014). Since the proximal His-Fe bond in mHb is unstable (Hargrove *et al.*, 1994), the hematin was thought to easily dissociate from mHb as the precursor to form ZnPP (Table 3, Fig. 16, 17A, and 18A). Consistently, the over-reduction in meat significantly suppressed ZnPP formation (Fig. 21), which was implied to mainly suppress the hematin dissociation from mHb by inhibiting the autoxidation of Hb. On the other hand, the heme scavenging system for the Hb clearance to eliminate its cytotoxic was proposed to cause the hematin dissociated from mHb to form ZnPP and produce apo-Hb simultaneously (Wakamatsu, 2022). Notably, before the conversion of hematin to ZnPP, a reduction of the dissociated hematin to heme by the endogenous reductases in meat was indicated to be needed. This phenomenon was explained by the mammalian FECH showed only the ability to catalyze the removal of iron from heme to form PPIX as the ZnPP-forming precursor (Chau *et al.*, 2010). Also, without reduction, the free hematin could not convert to ZnPP catalyzed by the mammalian FECH *in vitro* experiment (Fig. 20). Therefore, Hb was the favorable substrate for ZnPP formation in meat, which was also due to the hematin was easily dissociated from the autoxidized mHb, and then converted to ZnPP after being reduced to heme by the meat-inherent reductases.

4.2. ZnPP-Hb is formed by inserting ZnPP into the apo-Hb in meat

After the heme mainly dissociated from the Hb to convert to ZnPP, a large amount of ZnPP-Hb was observed as the water-soluble ZnPP complex in the new experimental model (Fig. 5). As mentioned above, when the heme/hematin dissociated from the Hb and the autoxidized mHb due to their unstable heme-globin binding and the heme scavenging system rather than the proteolysis, the apo-Hb with a vacant heme pocket could produce simultaneously. ZnPP as the hydrophobic substance was proposed to insert into the vacant hydrophobic heme-binding pocket of apo-Hb to form the water-soluble ZnPP-Hb complex (Wakamatsu, 2022), and this insertion could occur in the absence of any enzyme (Fig. 11). Therefore, when heme/hematin dissociated from Hb/mHb and converted to ZnPP, the apo-Hb was simultaneously produced, and then ZnPP was non-enzymatically inserted into apo-Hb to form the ZnPP-Hb as the dominating water-soluble ZnPP complex in meat.

4.3. Nitrite inhibits ZnPP formation in meat by suppressing the dissociation of heme from heme proteins as well as the degradation of a [2Fe-2S] cluster in FECH

To elucidate the heme destabilization in the heme-globin structure of heme proteins was significant for ZnPP formation in meat, more evidence for the changes in heme-globin binding stability of heme proteins and their corresponding heme dissociation amount during anaerobic incubation was needed. It has been reported that the nitrite, which was added to the common cured meat products, suppressed ZnPP formation in pork homogenate (Wakamatsu *et al.*, 2010). This phenomenon might be related to the NO derived from nitrite as the heme ligand bound to the heme iron of meat-endogenous heme proteins to form the nitrosyl heme proteins (Fig. 15A). When nitrite added to the raw meat, NO could bind with heme iron of the meat-endogenous Mb to form the stable NO-heme complex in NOMb (Wang *et al.*, 2018), which bring a long-lasting, bright red color for the nitrite-added cured meat (Honikel, 2008). Thus, the heme in NOMb was thought to be hard to dissociate from its heme pocket as the precursor to form ZnPP in nitrite-cured meat. In addition, NO could rapidly associate with the ferrous iron of heme (Fe^{2+}) located in the α and β subunits of the Hb to form the NOHb (Yi *et al.*, 2008). Meanwhile, after the Hb autoxidized to the mHb, NO could also bind to the ferric ion of mHb (Fe^{3+}) to

form the NOHb, which showed almost no pronounced distortion of the NO-hematin and maintained structural stability (Deatherage *et al.*, 1979). These binding conformations provided a stable heme/hematin-globin structure of NOHb under anaerobic conditions (Fig. 17B and 18B), and less heme/hematin could dissociate form its heme pocket as the precursor to form ZnPP *via* PPIX (Table 3, Fig. 16). Notably, since the mammalian FECH contains a NO-sensitive [2Fe-2S] cluster (Furukawa *et al.*, 1995; Sellers *et al.*, 1996; Weerth *et al.*, 2021), and the mammalian FECH was proposed to catalyze the conversion of heme to ZnPP in meat (Chau *et al.*, 2010), the NO degraded the [2Fe–2S] cluster of FECH to suppress its catalytic activity was proposed as one of the pathways by which nitrite inhibited ZnPP formation in meat (Wakamatsu *et al.*, 2010). Therefore, in addition to inactivating the mammalian FECH by degrading its [2Fe–2S] cluster, the nitrite could inhibit ZnPP formation in meat by deriving NO binding with meat-endogenous heme proteins to suppress heme dissociated from the stable heme-globin structure in nitrosyl heme proteins as ZnPP-forming precursor.

4.4. The potential formation pathway of the ZnPP-Mb in meat

As mentioned above, Mb was usually proposed as the main substrate to provide heme to convert to ZnPP in dry-cured meat products (Khozroughi *et al.*, 2019; Møller *et al.*, 2003), owing to its having the highest concentration in meat compared with Hb (Ledward, 1992). Also, the heme content of Mb was approximately twice of that of Hb in pork (Ledward, 1992). Moreover, since the concentration of ZnPP constituted 60-70% of the total porphyrin in Parma ham (Taketani *et al.*, 2007; Wakamatsu *et al.*, 2009), Mb was thought to be involved in the ZnPP formation in Parma ham because even if all the heme in Hb was converted to ZnPP, it was still lower than the ZnPP content in Parma ham. However, different from Hb, the addition of Mb had no supplemental effect on ZnPP formation in the experimental model as well as no ZnPP-Mb complex was observed in the new experimental model after 20 days anaerobic incubation (Fig. 5 and 8). This phenomenon could be explained by the heme dissociating from Mb as the ZnPP-forming precursor more slowly than from Hb in meat. The heme-globin binding of Mb was highly stable because the heme-7-propionate in Mb could link to the nearby surface amino acids residues to form a stable hydrogen bonding lattice (Hunter *et al.*, 1997; Ledward, 1992).

Thus, Mb could maintain the heme-globin binding compared with Hb under anaerobic conditions (Fig. 9 and 10), which resulted in the heme dissociation from the heme pocket of Mb was much lower than that of Hb (Fig. 8C). Meanwhile, due to less heme dissociated from Mb as the precursor to form ZnPP, the production of the apo-Mb might be slight. In addition, although the autoxidation of Mb occurred (Cai *et al.*, 2016), metMb can be quickly reduced *via* enzymatic, non-enzymatic, and electron-transport pathways in meat (Ramanathan *et al.*, 2020). Thus, it was thought that the hematin dissociated from the autoxidized metMb and the co-produced apo-Mb was negligible. Since the heme dissociation from Mb and the production of apo-Mb might be more difficult than those of Hb, the formation of ZnPP-Mb, which was speculated as non-enzymatically inserting ZnPP into apo-Mb, might be much slower than the formation of ZnPP-Hb in meat. Consistently, it has been reported that the amount of ZnPP-Hb complex was around 3-fold higher than ZnPP-Mb complex in Parma ham (Wang et al., 2021). However, since the incubation period of the new experimental model was only 20 days at the longest, much shorter than Parma ham, which needs to prepare over one year, almost no ZnPP-Mb was observed in the new experimental model (Fig. 5). It is possible that prolonging the incubation time will make the new experimental model produce the ZnPP-Mb. Therefore, since the heme dissociated from Mb to convert ZnPP and the simultaneous production of apo-Mb were thought to be very slow, the formation of ZnPP-Mb by non-enzymatically inserting ZnPP into apo-Mb might be little in meat with a short maturing period.

4.5. The suggested pathway for the water-soluble ZnPP formation in nitrite/nitrate-free dry-cured meat products

In summary, according to the results in the present study and those from the previously reported studies, the suggested formation pathway for the water-soluble ZnPP complexes in nitrite/nitrate-free dry-cured meat products was shown in Fig. 23. Although Mb is the most abundant heme proteins in meat, ZnPP was proposed mainly formed from Hb rather than Mb and existed as the ZnPP-Hb in the nitrite/nitrate-free dry-cured meat products. Since the heme-globin binding of Mb was stable, the heme dissociation from Mb was thought to be very slow and less apo-Mb could produce simultaneously. Also, the

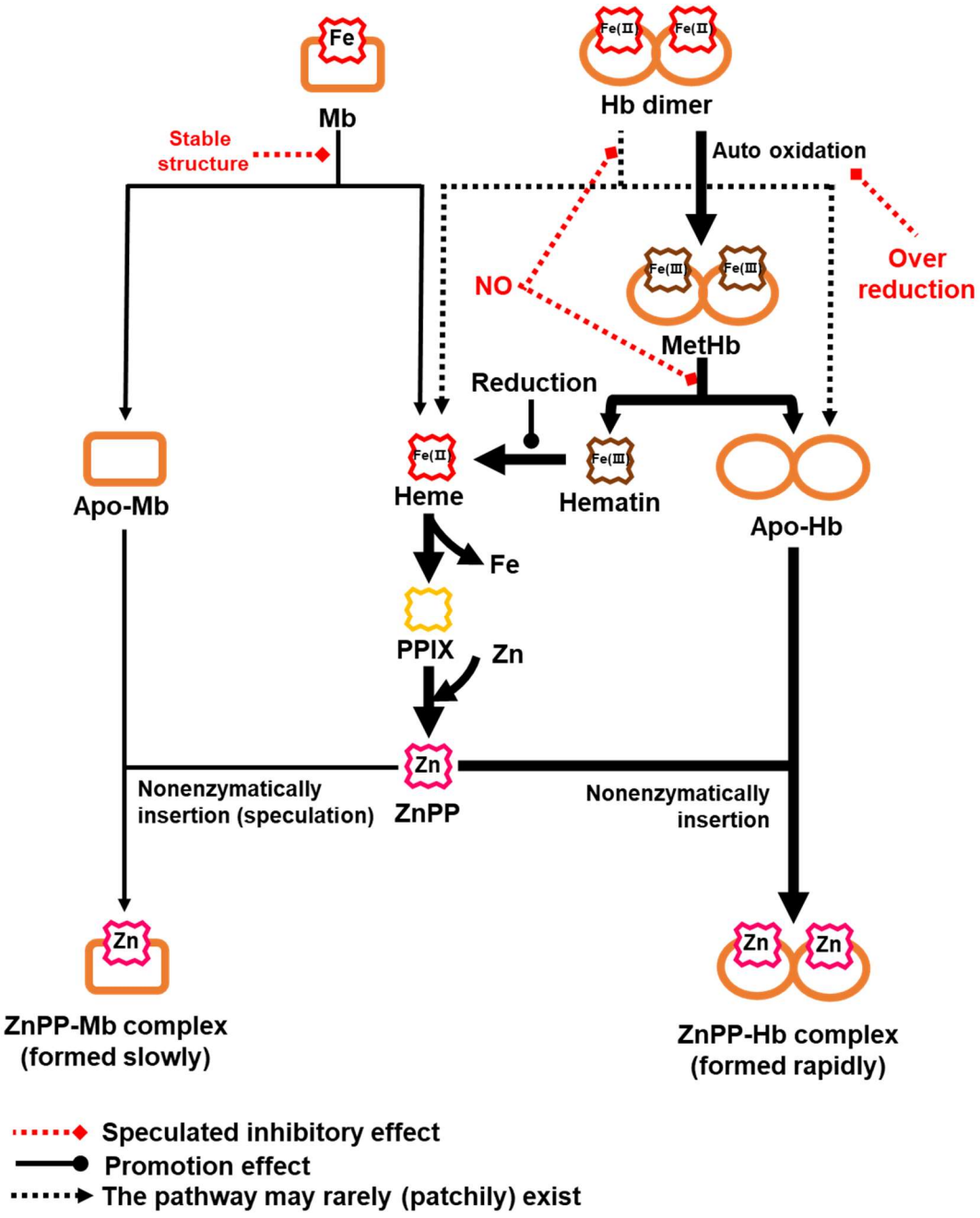

Fig. 23. The suggested pathway for the water-soluble ZnPP formation in nitrite/nitrate-free dry-cured meat products

ZnPP: Zinc protoporphyrin IX; PPIX: Protoporphyrin IX; NO: Nitric oxide; Line thickness indicates the degree of relevance.

autoxidized metMb could be rapidly reduced through various pathways in meat, thereby less hematin was thought to dissociate from the hematin-globin binding of metMb and the simultaneous production of apo-Mb might be negligible. Thus, the ZnPP-Mb complex, which was speculated as non-enzymatically inserting ZnPP into apo-Mb, might form slowly and exist in a small amount in the nitrite/nitrate-free dry-cured meat products with short maturation time. In contrast, the Hb that entered the muscle tissue dissociated a large amount of heme due to its unstable heme-globin binding and derived apo-Hb simultaneously. Meanwhile, the rapid autoxidation of Hb in meat resulted in hematin being easily dissociated from the autoxidized mHb. After the dissociated hematin from mHb was reduced to heme by the meat-inherent reductase, the free heme including the directly dissociated part was converted ZnPP *via* PPIX. Subsequently, the ZnPP-Hb, which was formed by non-enzymatically inserting ZnPP into apo-Hb, could rapidly produce and as the dominating water-soluble ZnPP complexes in the nitrite/nitrate-free dry-cured meat products.

Chapter 5

Abstract

This study was carried out to investigate the formation mechanism of the water-soluble ZnPP, which was the main ZnPP existence state in Parma ham, in the nitrite/nitrate-free dry-cured meat products using a newly established experimental model. First, a new experimental model to produce higher amount of water-soluble ZnPP complexes was optimized. Mainly the water-soluble ZnPP complex formed in this model was ZnPP-Hb dimer and was the same as that in Parma ham, indicating this new experimental model was suitable for studying the formation of water-soluble ZnPP. The addition of the exogenous Hb in the new model promoted higher ZnPP formation and released non-heme iron content than with Mb added, and the heme-globin binding stability of Hb was lower than that of Mb under the anaerobic conditions. These results indicated that compared with Mb, Hb may be easy to release heme as the substrate to form ZnPP due to its unstable heme-globin binding and may simultaneously produce apo-Hb. After only mixing the apo-Hb solution with the ZnPP standard, the ZnPP-Hb complex was formed, indicating ZnPP-Hb could form by non-enzymatically inserting ZnPP into the apo-Hb. As for ZnPP-Mb, its formation pathway is speculated to be similar to that of ZnPP-Hb, but the stable heme-globin binding of Mb may result in its less heme dissociation, leading to less ZnPP-Mb formation. On the other hand, the exogenous Hb could bind with the NO, which was derived from nitrite, to form NOHb. The NOHb showed a more stable heme-globin structure and lower heme dissociation amount during anaerobic incubation compared with the exogenous OxyHb. Also, the exogenous addition of NOHb to the experimental model had no supplemental effect on ZnPP formation. These results indicated that the NOHb was hard to dissociate heme to convert to ZnPP due to its stable heme-globin binding. Moreover, after the hematin released from the Hb and mHb, it needs previously reduce to heme and then converted to ZnPP. In contrast, the excessive reductant addition to the meat homogenate significantly suppressed the formation of ZnPP, which may because the over reduction suppressed the heme protein autoxidation, further limited their hematin dissociation. In conclusion, Hb was the dominating substrate to form ZnPP

because heme/hematin was easy to dissociate from Hb and autoxidized mHb due to their unstable heme-globin binding, and produced apo-Hb simultaneously. After the dissociated hematin was reduced to heme, the heme mainly dissociated from Hb was converted to ZnPP, followed by non-enzymatically inserting into apo-Hb to form the ZnPP-Hb complex in the nitrite/nitrate-free dry-cured meat products.

Acknowledgements

This thesis is a gift for my three-year Ph.D. career. After getting a master's degree, to pursue a better education, I came to Japan to study for my Ph.D. at Hokkaido University. The experience of international moves will be one of the most memorable things in my life. Through this studying journey, I learned a lot about food science and experienced a different culture.

Upon the completion of this dissertation, I am grateful to those who have offered me encouragement and support during my doctoral study at Hokkaido University.

First of all, I extend my deepest gratitude to my supervisor Associate Professor Jun-ichi Wakamatsu. He has offered me the opportunity for studying at the Laboratory of Applied Food Science, Hokkaido University. His suggestions will be a valuable asset for my future academic study.

I deeply appreciate Professor Haruto Kumura for reviewing my dissertation and for his encouragement and valuable suggestions during my study at Hokkaido University. I sincerely appreciate Professor Takafumi Gotoh and Assistant Professor Toru Hayakawa for reviewing the dissertation and for his valuable comments.

I am grateful to my supervisor Professor Ming Huang at Nanjing Agricultural University, during my master course. Without his suggestion, I would not have proceeded to doctoral study.

I sincerely appreciate Dr. Hung-Cheng Wang and Ms. Haruka Abe for their kind help during my experiments and the spiritually powerful encouragement during my thesis writing.

Particular thanks go to every member in the Laboratory of Applied Food Science, Hokkaido University for their kind help and encouragement.

I would like to thank the Chinese Scholarship Council and Japanese Government Scholarship for giving me this valuable opportunity to study abroad and for the financial support.

Finally, my dearest family gave me the most reliable backing. My mother, my father, and my wife, I love you.

References

Abril, B., Sanchez-Torres, E. A., Bou, R., Garcia-Perez, J. V., & Benedito, J. (2021). Ultrasound intensification of Ferrochelatase extraction from pork liver as a strategy to improve zinc-protoporphyrin formation. *Ultrasonics Sonochemistry*, *78*, 105703.

Adamsen, C. E., Møller, J. K., Hismani, R., & Skibsted, L. H. (2004). Thermal and photochemical degradation of myoglobin pigments in relation to colour stability of sliced dry-cured Parma ham and sliced dry-cured ham produced with nitrite salt. *European Food Research and Technology*, *218*(5), 403–409.

Adamsen, C. E., Møller, J. K., Laursen, K., Olsen, K., & Skibsted, L. H. (2006). Zn-porphyrin formation in cured meat products: Effect of added salt and nitrite. *Meat Science*, *72*(4), 672–679.

Ahn, D. U., Wolfe, F. H., & Sim, J. S. (1993). Three Methods for Determining Nonheme Iron in Turkey Meat. *Journal of Food Science*, *58*(2), 288–291.

Alahakoon, A. U., Jayasena, D. D., Ramachandra, S., & Jo, C. (2015). Alternatives to nitrite in processed meat: Up to date. *Trends in Food Science & Technology*, *45*(1), 37–49.

Alben, J. O., & Fager, L. Y. (1972). Infrared studies of azide bound to myoglobin and hemoglobin temperature dependence of ionicity. *Biochemistry*, *11*(5), 842–847.

Ascenzi, P., Bocedi, A., Visca, P., Altruda, F., Tolosano, E., Beringhelli, T., & Fasano, M. (2005). Hemoglobin and heme scavenging. *IUBMB Life*, *57*(11), 749–759.

Becker, E. M., Westermann, S., Hansson, M., & Skibsted, L. H. (2012). Parallel enzymatic and non-enzymatic formation of zinc protoporphyrin IX in pork. *Food Chemistry*, *130*(4), 832–840.

Bedale, W., Sindelar, J. J., & Milkowski, A. L. (2016). Dietary nitrate and nitrite: Benefits, risks, and evolving perceptions. *Meat Science*, *120*, 85–92.

Boles, J. A., & Pegg, R. (2010). Meat color. *Montana State University and Saskatchewan Food Product Innovation, Program University of Saskatchewan*.

Bouvard, V., Loomis, D., Guyton, K. Z., Grosse, Y., El Ghissassi, F., Benbrahim-Tallaa, L., Guha, N., Mattock, H., & Straif, K. (2015). Carcinogenicity of consumption of red and processed meat. *The Lancet Oncology*, *16*(16), 1599–1600.

Cai, H., Tatiyaborworntham, N., Yin, J., & Richards, M. P. (2016). Assessing low redox stability of myoglobin relative to rapid hemin loss from hemoglobin: oxidative degradation of Hb and Mb. *Journal of Food Science*, *81*(1), C42–C48.

Cantwell, M., & Elliott, C. (2017). Nitrates, nitrites and nitrosamines from processed meat intake and colorectal cancer risk. *The American Journal of Clinical Nutrition*, *3*(4), 27-31.

Carey, C. C. (2020). United States food and drug administration. In *Clinical Engineering Handbook* (pp. 764–773). Elsevier.

Carpenter, C. E., Cornforth, D. P., & Whittier, D. (2001). Consumer preferences for beef color and packaging did not affect eating satisfaction. *Meat Science*, *57*(4), 359–363.

Chau, T. T., Ishigaki, M., Kataoka, T., & Taketani, S. (2010). Porcine ferrochelatase: The relationship between iron-removal reaction and the conversion of heme to Zn-protoporphyrin. *Bioscience, Biotechnology, and Biochemistry*, *74*(7), 1415–1420.

Chau, T. T., Ishigaki, M., Kataoka, T., & Taketani, S. (2011). Ferrochelatase catalyzes the formation of Zn-protoporphyrin of dry-cured ham via the conversion reaction from heme in meat. *Journal of Agricultural and Food Chemistry*, *59*(22), 12238–12245.

De Maere, H., Chollet, S., Claeys, E., Michiels, C., Govaert, M., De Mey, E., Paelinck, H., & Fraeye, I. (2017). *In vitro* zinc protoporphyrin IX formation in different meat sources related to potentially important intrinsic parameters. *Food and Bioprocess Technology*, *10*(1), 131–142.

De Maere, H., Fraeye, I., De Mey, E., Dewulf, L., Michiels, C., Paelinck, H., & Chollet, S. (2016). Formation of naturally occurring pigments during the production of nitrite-free dry fermented sausages. *Meat Science*, *114*, 1–7.

Deatherage, J. F., Obendorf, S. K., & Moffat, K. (1979). Structure of azide methemoglobin. *Journal of Molecular Biology*, *134*(3), 419–429.

Flores, M., & Toldrá, F. (2021). Chemistry, safety, and regulatory considerations in the use of nitrite and nitrate from natural origin in meat products-Invited review. *Meat Science*, *171*, 108272.

Furukawa, T., Kohno, H., Tokunaga, R., & Taketani, S. (1995). Nitric oxide-mediated inactivation of mammalian ferrochelatase *in vivo* and *in vitro*: Possible involvement of the iron-sulphur cluster of the enzyme. *Biochemical Journal*, *310*(2), 533–538.

Ghadiri Khozroughi, A., Braga, T. W., Wagner, J., & Rawel, H. (2019). Investigation of the post mortem zinc protoporphyrin IX fluorescence with respect to its protein-bound and unbound occurrence in aqueous meat extracts. *Food Chemistry*, *283*(15), 462–467.

Ghadiri Khozroughi, A., Kroh, L. W., Schlüter, O., & Rawel, H. (2018). Assessment of the bacterial impact on the post-mortem formation of zinc protoporphyrin IX in pork meat. *Food Chemistry*, *256*(1), 25–30.

Grossi, A. B., do Nascimento, E. S., Cardoso, D. R., & Skibsted, L. H. (2014). Proteolysis involvement in zinc–protoporphyrin IX formation during Parma ham maturation. *Food Research International*, *56*, 252–259.

Gyulkhandanyan, A., Gyulkhandanyan, L., Ghazaryan, R., Fleury, F., Angelini, M., Gyulkhandanyan, G., & Sakanyan, V. (2013). Assessment of new cationic porphyrin binding to plasma proteins by planar microarray and spectroscopic methods. *Journal of Biomolecular Structure and Dynamics*, *31*(4), 363–375.

Hargrove, M. S., Singleton, E. W., Quillin, M. L., Ortiz, L. A., Phillips Jr, G. N., Olson, J. S., & Mathews, A. J. (1994). His64 (E7)–> Tyr apomyoglobin as a reagent for measuring rates of hemin dissociation. *Journal of Biological Chemistry*, *269*(6), 4207–4214.

Hargrove, M. S., Whitaker, T., Olson, J. S., Vali, R. J., & Mathews, A. J. (1997). Quaternary structure regulates hemin dissociation from human hemoglobin. *Journal of Biological Chemistry*, *272*(28), 17385–17389.

Honikel, K.-O. (2008). The use and control of nitrate and nitrite for the processing of meat products. *Meat Science*, *78*(1–2), 68–76.

Huang, Y.-X., Wu, Z.-J., Huang, B.-T., & Luo, M. (2013). Pathway and Mechanism of pH Dependent Human Hemoglobin Tetramer-Dimer-Monomer Dissociations. *PLoS ONE*, *8*(11), e81708.

Hunter, C. L., Lloyd, E., Eltis, L. D., Rafferty, S. P., Lee, H., Smith, M., & Mauk, A. G. (1997). Role of the Heme Propionates in the Interaction of Heme with Apomyoglobin and Apocytochrome b_5. *Biochemistry*, *36*(5), 1010–1017.

Jin, S.-K., Choi, J.-S., Moon, S.-S., Jeong, J.-Y., & Kim, G.-D. (2014). The assessment of red beet as a natural colorant, and evaluation of quality properties of emulsified pork sausage containing red beet powder during cold storage. *Korean Journal for Food Science of Animal Resources*, *34*(4), 472-481.

Kranen, R. W., Van Kuppevelt, T. H., Goedhart, H. A., Veerkamp, C. H., Lambooy, E., & Veerkamp, J. H. (1999). Hemoglobin and myoglobin content in muscles of broiler chickens. *Poultry Science*, *78*(3), 467–476.

Laursen, K., Adamsen, C. E., Laursen, J., Olsen, K., & Møller, J. K. (2008). Quantification of zinc–porphyrin in dry-cured ham products by spectroscopic methods: Comparison of absorption, fluorescence and X-ray fluorescence spectroscopy. *Meat Science*, *78*(3), 336–341.

Ledward, D. A. (1992). Haemoproteins in meat and meat products. In *Biochemistry of food proteins* (pp. 197–234). Springer.

Lee, S. Y., Jo, C., Yoon, Y., Jeong, J. Y., & Hur, S. J. (2021). Effect on health from consumption of meat and meat products. *Journal of Animal Science and Technology*, *63*(5), 955-976.

Love, J. D., & Pearson, A. M. (1974). Metmyoglobin and nonheme iron as prooxidants in cooked meat. *Journal of Agricultural and Food Chemistry*, *22*(6), 1032–1034.

Ma, X., Sun, Y., Pan, D., Cao, J., & Dang, Y. (2022). Structural characterization and stability analysis of phosphorylated nitrosohemoglobin. *Food Chemistry*, *373*, 131475.

Mancini, R. A., & Hunt, Mc. (2005). Current research in meat color. *Meat Science*, *71*(1), 100–121.

Møller, J. K., Adamsen, C. E., Catharino, R. R., Skibsted, L. H., & Eberlin, M. N. (2007). Mass spectrometric evidence for a zinc–porphyrin complex as the red pigment in

dry-cured Iberian and Parma ham. *Meat Science*, *75*(2), 203–210.

Møller, J. K., Adamsen, C. E., & Skibsted, L. H. (2003). Spectral characterisation of red pigment in Italian-type dry-cured ham. Increasing lipophilicity during processing and maturation. *European Food Research and Technology*, *216*(4), 290–296.

Morita, H., Niu, J., Sakata, R., & Nagata, Y. (1996). Red pigment of Parma ham and bacterial influence on its formation. *Journal of Food Science*, *61*(5), 1021–1023.

W. H. O. (2017). Evaluations of the Joint FAO. *WHO Expert Committee on Food Additives*.

Parolari, G., Aguzzoni, A., & Toscani, T. (2016). Effects of processing temperature on color properties of dry-cured hams made without nitrite. *Foods*, *5*(2), 33-47.

Parthasarathy, D. K., & Bryan, N. S. (2012). Sodium nitrite: The “cure” for nitric oxide insufficiency. *Meat Science*, *92*(3), 274–279.

Pennell, R. B. (1964). Composition of normal human red cells. *The Red Blood Cell*, *1*, Chapter 3, 93-135.

Radi, R. (1996). Reactions of nitric oxide with metalloproteins. *Chemical Research in Toxicology*, *9*(5), 828–835.

Ramanathan, R., Suman, S. P., & Faustman, C. (2020). Biomolecular Interactions Governing Fresh Meat Color in Post-mortem Skeletal Muscle: A Review. *Journal of Agricultural and Food Chemistry*, *68*(46), 12779–12787.

Rivera, N., Bunning, M., & Martin, J. (2019). Uncured-labeled meat products produced using plant-derived nitrates and nitrites: Chemistry, safety, and regulatory considerations. *Journal of Agricultural and Food Chemistry*, *67*(29), 8074–8084.

Sakaino, M., Ishigaki, M., Ohgari, Y., Kitajima, S., Masaki, R., Yamamoto, A., & Taketani, S. (2009). Dual mitochondrial localization and different roles of the reversible reaction of mammalian ferrochelatase: Mitochondrial location of ferrochelatase. *FEBS Journal*, *276*(19), 5559–5570.

Santarelli, R. L., Pierre, F., & Corpet, D. E. (2008). Processed meat and colorectal cancer: A review of epidemiologic and experimental evidence. *Nutrition and Cancer*, *60*(2), 131–144.

Sato, K., & Hegarty, G. R. (1971). Warmed-over flavor in cooked meats. *Journal of Food Science*, *36*(7), 1098–1102.

Schaer, D. J., Vinchi, F., Ingoglia, G., Tolosano, E., & Buehler, P. W. (2014). Haptoglobin, hemopexin, and related defense pathways—Basic science, clinical perspectives, and drug development. *Frontiers in Physiology*, *5*, 415.

Sebranek, J. G., & Bacus, J. N. (2007). Cured meat products without direct addition of nitrate or nitrite: What are the issues? *Meat Science*, *77*(1), 136–147.

Sellers, V. M., Johnson, M. K., & Dailey, H. A. (1996). Function of the [2Fe− 2S] cluster in mammalian ferrochelatase: A possible role as a nitric oxide sensor. *Biochemistry*, *35*(8), 2699–2704.

Shimizu, T., Huang, D., Yan, F., Stranava, M., Bartosova, M., Fojtíková, V., & Martínková, M. (2015). Gaseous O_2, NO, and CO in signal transduction: Structure and function relationships of heme-based gas sensors and heme-redox sensors. *Chemical Reviews*, *115*(13), 6491–6533.

Sindelar, J. J., & Milkowski, A. L. (2011). Sodium nitrite in processed meat and poultry meats: A review of curing and examining the risk/benefit of its use. *American Meat Science Association White Paper Series*, *3*, 1–14.

Taketani, S., Ishigaki, M., Mizutani, A., Uebayashi, M., Numata, M., Ohgari, Y., & Kitajima, S. (2007). Heme synthase (ferrochelatase) catalyzes the removal of iron from heme and demetalation of metalloporphyrins. *Biochemistry*, *46*(51), 15054–15061.

Tomasevic, I., Djekic, I., Font-i-Furnols, M., Terjung, N., & Lorenzo, J. M. (2021). Recent advances in meat color research. *Current Opinion in Food Science*, *41*, 81–87.

Wakamatsu, J. (2022). Evidence of the mechanism underlying zinc protoporphyrin IX formation in nitrite/nitrate-free dry-cured Parma ham. *Meat Science*, *192*, 108905.

Wakamatsu, J., Akter, M., Honma, F., Hayakawa, T., Kumura, H., & Nishimura, T. (2019). Optimal pH of zinc protoporphyrin IX formation in porcine muscles: Effects of muscle fiber type and myoglobin content. *LWT - Food Science and Technology*, *101*, 599–606.

Wakamatsu, J., Hayashi, N., Nishimura, T., & Hattori, A. (2010). Nitric oxide inhibits the formation of zinc protoporphyrin IX and protoporphyrin IX. *Meat Science*, *84*(1), 125–128.

Wakamatsu, J., Nishimura, T., & Hattori, A. (2004a). A Zn–porphyrin complex contributes to bright red color in Parma ham. *Meat Science*, *67*(1), 95–100.

Wakamatsu, J., Odagiri, H., Nishimura, T., & Hattori, A. (2009). Quantitative determination of Zn protoporphyrin IX, heme and protoporphyrin IX in Parma ham by HPLC. *Meat Science*, *82*(1), 139–142.

Wakamatsu, J., Okui, J., Hayashi, N., Nishimura, T., & Hattori, A. (2007). Zn protoporphyrin IX is formed not from heme but from protoporphyrin IX. *Meat Science*, *77*(4), 580–586.

Wakamatsu, J., Okui, J., Ikeda, Y., Nishimura, T., & Hattori, A. (2004b). Establishment of a model experiment system to elucidate the mechanism by which Zn–protoporphyrin IX is formed in nitrite-free dry-cured ham. *Meat Science*, *68*(2), 313–317.

Wang, B., Shi, Y., Tejero, J., Powell, S. M., Thomas, L. M., Gladwin, M. T., Shiva, S., Zhang, Y., & Richter-Addo, G. B. (2018). Nitrosyl myoglobin and their nitrite precursors: crystal structural and QM/MM theoretical investigations into preferred Fe–NO ligand orientations in myoglobin distal pockets. *Biochemistry*, *57*(32), 4788-4802.

Wang, H.-C., Hayakawa, T., Kumura, H., & Wakamatsu, J. (2021). Water-extractable zinc protoporphyrin IX in Parma ham predominantly exists as complexes with hemoglobin and myoglobin. *Food Bioscience*, *40*, 100870.

Warriss, P. D. (1977). The residual blood content of meat—A review. *Journal of the Science of Food and Agriculture*, *28*(5), 457–462.

Weerth, R. S., Medlock, A. E., & Dailey, H. A. (2021). Ironing out the distribution of [2Fe-2S] motifs in ferrochelatases. *Journal of Biological Chemistry*, *297*(5), 101017.

Xu, P., Zhu, X., Tan, S., Qin, H., & Zhou, C. (2016). The role of monoxide hemoglobin in color improvement of chicken sausage. *Food Science and Biotechnology*, *25*(2), 409–414.

Yi, J., Safo, M. K., & Richter-Addo, G. B. (2008). The nitrite anion binds to human hemoglobin via the uncommon O-nitrito mode. *Biochemistry*, *47*(32), 8247–8249.

王鴻誠. (2020). 乾塩漬食肉製品における亜鉛プロトポルフィリン IX 形成機構に関する研究: 形成経路と水溶性 ZnPP 複合体の解明. 北海道大学大学院農学研究院　博士論文.